CANCER

A cross-talk established by tumor-targeted cytokines rescues CAR T cell activity and engages host T cells against glioblastoma in mice

Federico Rossari[1,2]†, Giorgia Alvisi[1]†, Melania Cusimano[1], Stefano Beretta[1,2], Filippo Birocchi[1,2]‡, Deborah I. Ambrosecchia[1], Ottavia Vitaloni[1], Chiara Brombin[3], Paola Maria Vittoria Rancoita[3], Tamara Canu[4], Giorgio Orofino[1,2], Andrea Annoni[1], Bernhard Gentner[1]§, Mario Leonardo Squadrito[1], Marco Genua[1], Renato Ostuni[1,2], Ivan Merelli[1,5], Nadia Coltella[1]*¶, Luigi Naldini[1,2]*¶

Chimeric antigen receptor (CAR) T cells have shown limited efficacy against solid tumors because of poor tissue penetration, constrained activity, and early exhaustion due to the immunosuppressive tumor microenvironment (TME). Although stimulatory cytokines can counteract immune suppression, their systemic administration entails risk of toxicities and counter-regulatory responses. Here, we leveraged a population of tumor-associated TIE2-expressing macrophages (TEMs) to release interferon-α (IFN-α) and/or orthogonal interleukin-2 (oIL2) at the tumor site. Targeted cytokine delivery rescued CAR T cell functionality against the clinically relevant tumor antigen B7-homolog 3 (B7-H3) in an orthotopic, CAR T cell–refractory, immunocompetent mouse model of glioblastoma (GBM) named mGB2 that recapitulates pathological features of the human disease. Immunophenotypic and transcriptomic analyses revealed that inhibition of premature terminal exhaustion and induction of effector and memory states featuring activation of signaling pathways and transcriptional networks putatively boosted CAR T cell antitumor activity. Furthermore, IFN-α, especially when combined with private oIL2 signaling to CAR T cells, elicited potent endogenous T cell responses against multiple tumor-associated antigens, leading to delayed GBM growth and prolonged mouse survival even with tumors expressing B7-H3 in only a fraction of cells. These data suggest that the combination of TEM-based cytokine delivery and CAR T cells may have synergistic effects and support the further study of this approach for the treatment of patients with GBM.

INTRODUCTION

Chimeric antigen receptor (CAR) T cells represent a pillar of immune therapy for hematological malignancies, but their therapeutic activity has been limited in solid tumors (*1*). Major roadblocks hindering CAR T cell activity in the tumor microenvironment (TME) include (i) limited homing and trafficking, (ii) limited persistence and proliferation, and (iii) induced dysfunction and exhaustion (*1*). In addition, CAR T cell–dependent toxicities and tumor escape mechanisms including immune evasion represent further challenges to successful clinical application (*1*).

A promising approach to potentiate CAR T cell function is to provide immune stimulatory cytokines to counteract some of the suppressive features of the TME (*2*). However, systemic or unregulated cytokine administration entails a high risk of toxicity and counter-regulatory mechanisms because of immune hyperactivation (*2*). To safely deliver cytokines at the tumor site, we established a clinical-grade platform leveraging a population of tumor-associated TIE2-expressing monocytes/macrophages (TEMs) as vehicles (*3*, *4*). This myeloid subset is consistently found at low and variable frequency in most tumor types and has been associated with tumor angiogenesis, therapy resistance, and metastasis, thus representing a broadly applicable candidate for drug delivery to a progressing tumor (*4*). We engineered hematopoietic stem cells (HSCs) with lentiviral vectors (LVs) expressing the cytokine of interest under the *Tie2* gene transcriptional regulation. MicroRNA target sequences (miRTs) were also added to prevent transgene expression from TIE2-expressing HSCs, thus limiting cytokine expression in the bone marrow (BM) and enabling selective expression in their TEM progeny (*3*–*6*). This strategy allowed cytokine-dependent antitumor responses in different tumor models (*6*–*8*) and is currently under clinical testing in a phase 1/2a trial in patients with glioblastoma (GBM) (Temferon NCT03866109, clinicaltrials.gov, Genenta Science).

GBM is a paradigmatic example of an "immune desert" tumor because of minimal infiltration and persistence of activated T cells, which generally acquire dysfunctional states including anergy, tolerance, senescence, and exhaustion (*9*). In contrast, myeloid cells mainly with protumoral and immunosuppressive features heavily infiltrate the tumor (*10*). This hostile TME strongly contributes to GBM's poor prognosis and likely represents the main cause for inadequate efficacy of immunotherapeutic strategies including immune checkpoint blockers and CAR T cells (*11*). In a murine syngeneic GBM model recapitulating the histopathological features of human disease (*12*), we showed that targeted delivery of

[1]San Raffaele Telethon Institute for Gene Therapy (SR-Tiget), IRCCS San Raffaele Scientific Institute, 20132 Milan, Italy. [2]Vita-Salute San Raffaele University, 20132 Milan, Italy. [3]CUSSB-University Center for Statistics in the Biomedical Sciences, Vita-Salute San Raffaele University, 20132 Milan, Italy. [4]Experimental Imaging Center, Preclinical Imaging Facility, IRCCS San Raffaele Scientific Institute, 20132 Milan, Italy. [5]National Research Council, Institute for Biomedical Technologies, 20054 Segrate, Italy.
†These authors contributed equally to this work.
‡Present address: Cancer Center, Massachusetts General Hospital and Harvard Medical School, Boston, MA 02115, USA.
§Present address: Ludwig Institute for Cancer Research and Department of Oncology, University of Lausanne (UNIL), and Lausanne University Hospital (CHUV), Lausanne 1011, Switzerland.
*Corresponding author. Email: coltella.nadia@hsr.it (N.C.); naldini.luigi@hsr.it (L.N.)
¶These authors contributed equally to this work.

interferon-α (IFN-α) by TEMs counteracted tumor growth with concomitant changes in the immune microenvironment, including the loss of a population of tumor-associated macrophages (TAMs) whose gene signature is associated with protumoral functions and predicts poor prognosis of patients with GBM (*7*).

Because the immunosuppressive TME is a key hurdle for effective CAR T cell therapy, changes in the TME mediated by IFN-α gene therapy could generate a more favorable milieu for their function. Moreover, the possibility to support CAR T cells with a paracrine, localized, and private release of other cytokines may constitute a powerful tool to potentiate adoptive T cells, reducing the risks of toxicity associated with exogenous cytokine administration and armored T cell products (*2*).

Here, we leveraged TME-targeted cytokine delivery to overcome the lack of efficacy of CAR T cells in solid tumors using a second-generation murine CAR carrying a B7-homolog 3 (B7-H3) antigen binding domain already deployed in clinical trials for solid tumors, including GBM, and showing high homology with the mouse counterpart (*13*, *14*).

RESULTS

Optimized manufacturing of murine CAR T cells allows efficient targeting of the clinically relevant B7-H3 antigen in a GBM model

We first established an optimized process for generation of murine CAR T cells. Murine T cells were transduced with a bidirectional LV (BdLV) encoding for the murine CAR and a truncated form of the low-affinity nerve growth factor receptor (ΔNGFR) as a marker of transduction (fig. S1A and table S1). The optimized process included T cell stimulation with αCD3 and αCD28 (α, anti-) monoclonal antibodies coated onto plates (fig. S1, B to D), followed by transduction with 20 LV transducing units (TU)/cell per ml 24 hours post-stimulation (fig. S1, E and F) in the presence of LentiBoost (*15*) (fig. S1G) and cyclosporin H (CsH), a nonimmunosuppressive cyclosporine that mitigates LV innate cellular sensing (*16*) (fig. S1, H and I). Overall, we obtained an average of 60% transduced murine T cells, without affecting the phenotypic composition or the proliferative capacity of cultured T cells (fig. S1, J to M).

Next, we identified surface mouse GBM antigens that are also expressed by human GBM and can be targeted by mouse CAR constructs sharing the same single-chain variable fragment (scFv) as human CARs already in clinical trials. To this aim, we used the mGB2 murine syngeneic GBM model, which closely resembles the human pathology (*12*) and which harbors TEMs within its TME accounting for up to 3% of the total cells (*7*). Transcriptomic and immunophenotypic analysis of mGB2 cells revealed high and homogeneous expression of B7-H3 (CD276) (fig. S2, A to F), which is currently being investigated as a CAR target in several GBM clinical trials (*17*).

We generated murine B7-H3 CAR (CAR_{B7H3}) incorporating the 376.96 scFv clone, which is known to recognize both murine and human B7-H3, albeit with higher affinity for the latter (*13*), into the BdLV backbone also encoding for the ΔNGFR (Fig. 1A). Coexpression of CAR and ΔNGFR after transduction was confirmed by flow cytometry (Fig. 1B). As a control, we generated a BdLV driving expression of a murine CAR comprising an scFv targeting the human CD19 (CAR_{hCD19}) (Fig. 1A), a B cell antigen not expressed by GBM cells. CAR_{B7H3} T cells specifically up-regulated the expression of both the activation marker CD69 and ΔNGFR when cultured with B7-H3–positive cells, whereas control CAR_{hCD19} T cells did not (fig. S3, A to D). Similarly, coculture with B7-H3–positive cells induced IFN-γ release, tumor cell elimination, and proliferation of CAR_{B7H3} T cells (fig. S3, E to G).

IFN-α gene therapy improves activation and mitigates exhaustion of $CAR_{B7\text{-}H3}$ T cells, enhancing antitumor activity

Once we validated both expression and functionality of CAR_{B7H3} in vitro, we tested it in mice transplanted with HSCs previously transduced with *Tie2-Ifna1-miRT* LV (hereafter referred to as IFN mice) or a control LV lacking the expression cassette (hereafter referred to as Empty mice) and orthotopically challenged with mGB2 cells (Fig. 1C). We performed multiple independent experiments with a total of 34 to 54 mice per experimental condition. Adoptive transfer of CAR_{B7H3} T cells, through systemic [upon lymphodepleting conditioning by cyclophosphamide (CPA)] and/or intratumoral injection, led to only minor reduction in tumor burden as assessed by magnetic resonance imaging (MRI) and lack of survival advantage over control CAR_{hCD19} T cells in Empty mice. The control CAR_{hCD19} T cells, in turn, did not provide any survival advantage or tumor inhibition compared to untransduced T cells (fig. S3, H to K). In contrast, IFN-α gene therapy, coupled with control CAR_{hCD19} T cells, displayed therapeutic benefit in terms of both tumor growth reduction and prolonged mouse survival (Fig. 1, D and E). When CAR_{B7H3} T cell treatment was combined with IFN-α gene therapy, a superior effect was achieved in both reduction of tumor burden and prolonged survival, lowering the risk of death by 85% [hazard ratio (HR) = 0.15; Fig. 1, D and E] and indicating robust antitumor effects from the adoptively transferred CAR T cells.

Among the fraction of longest surviving mice, one mouse treated with IFN-α gene therapy and CAR_{B7H3} T cells that cleared the tumor also rejected a tumor rechallenge with a B7-H3 knockout mGB2 line (B7-$H3^{-}$) able to form tumors in naïve wild-type (wt) mice (fig. S4, A and B). This suggested the potential for establishment of a broader protective immunity extended to tumor antigens beyond the CAR target.

One week after injection, systemically administered CAR_{B7H3} T cells circulated at lower concentration in the peripheral blood and displayed a more activated phenotype according to the early up-regulation of immune checkpoint receptors [ICRs: programmed cell death protein (PD-1), lymphocyte-activation gene 3 (LAG-3), and cytotoxic T-lymphocyte associated protein 4 (CTLA-4)] and interleukin 2 receptor alpha (IL2Rα or CD25), compared with CAR_{hCD19} T cells, without major differences between Empty and IFN mice (Fig. 1, F and G). Three weeks after systemic adoptive cell transfer, the tumor immune infiltrate of Empty and IFN mice, despite having no quantitative differences in lineage composition (fig. S4C), was enriched in CAR_{B7H3} T cells compared with CAR_{hCD19} T cells, suggesting a target antigen–driven trafficking or local expansion, possibly explaining their reduction in the periphery (Fig. 1H). CAR_{B7H3} T cells belonged almost completely to the $CD8^{+}$ subset, whereas CAR_{hCD19} T cells also comprised 10 to 20% $CD4^{+}$ cells (fig. S4D). IFN-α gene therapy enhanced the expression of effector and activation markers [granzyme B (GZMB), CD69, and CD44] and reduced the expression of ICRs on CAR_{B7H3} T cells (Fig. 1I and fig. S4E), significantly mitigating the development of exhausted cells highly coexpressing ICRs ($P = 0.0258$, Fig. 1J). No target antigen escape was detected in tumor cells (fig. S4F).

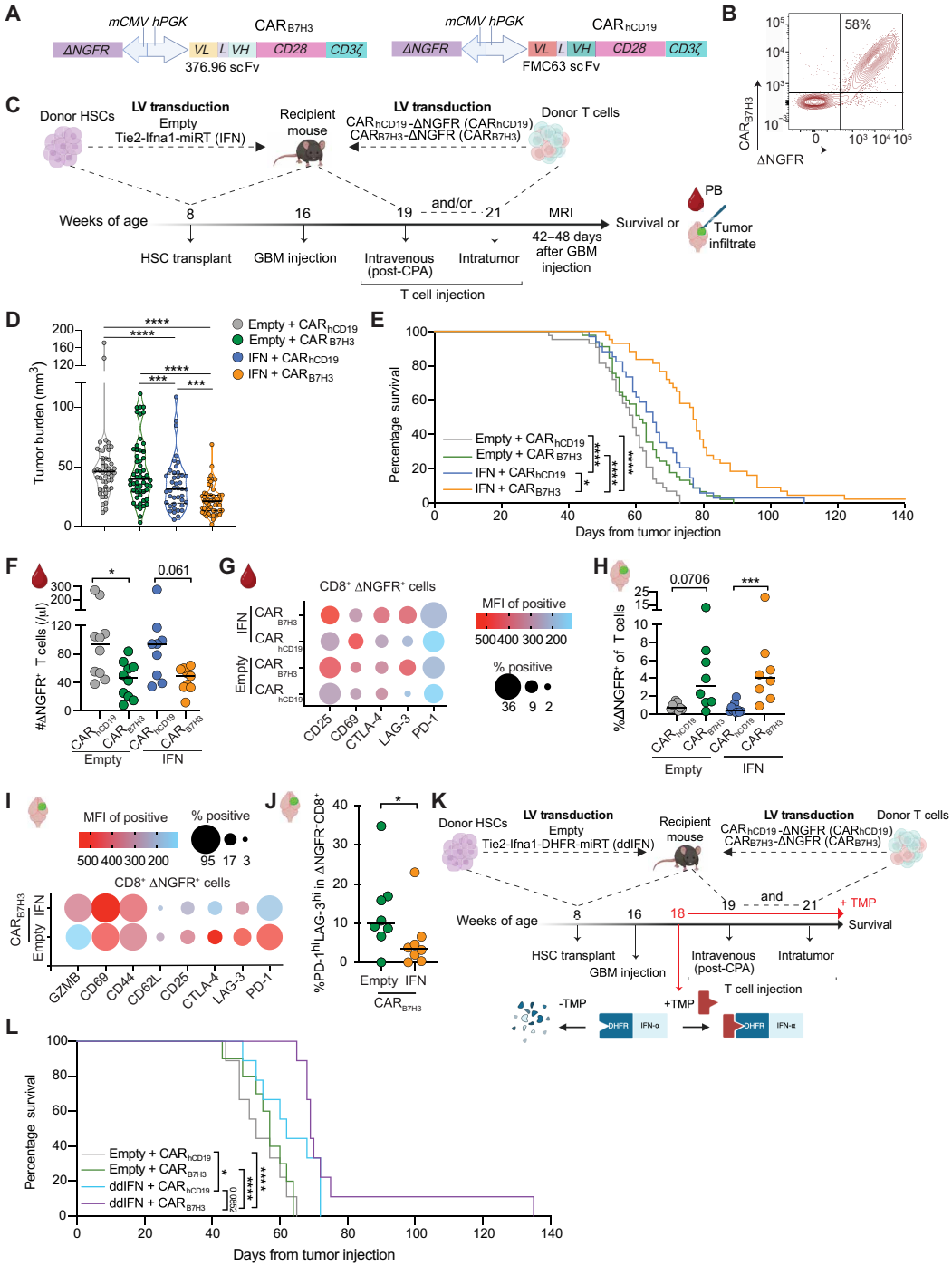

Fig. 1. Tumor-targeted IFN-α delivery improves $CAR_{B7\text{-}H3}$ T activation and reduces exhaustion, leading to rescued functionality and synergistic antitumor activity. (**A**) Schematic representation of the CAR_{B7H3}-ΔNGFR and CAR_{hCD19}-ΔNGFR BdLV constructs (VL, variable light chain; VH, variable heavy chain; L, linker; mCMV, minimal CMV promoter; PGK, phosphoglycerate kinase promoter). (**B**) Assessment of CAR_{B7H3} and ΔNGFR coexpression in transduced T cells by flow cytometry. (**C**) Experimental outline for treatment efficacy and mechanism evaluation: HSCs from donor mice were transduced with an empty (Empty) or Tie2-Ifna1-mirT LV vector (IFN) and transplanted into lethally irradiated C57BL/6 mice. After hematopoietic reconstitution, mGB2 cells were injected in the brain striatum. Mice received either CAR_{hCD19} or CAR_{B7H3} T cells intravenously upon lymphodepletion (ACT, adoptive cell transfer) and/or intratumorally. Tumor growth was monitored by MRI. Survival analysis and immunophenotype characterization of peripheral blood (PB) and tumor infiltrate were the end points of different experiments. (**D**) Tumor burden assessment by MRI 42 to 48 days after GBM injection (n = 7 independent experiments; n = 49, 54, 41, and 53 mice in Empty plus CAR_{hCD19}, Empty plus CAR_{B7H3}, IFN plus CAR_{hCD19}, and IFN plus CAR_{B7H3} groups, respectively; LME with random effects on experiment ID and administration route, see Materials and Methods). (**E**) Kaplan-Meier survival curves of mGB2-bearing mice in different treatment groups (n = 6 independent experiments; n = 43, 45, 34, and 42 mice in Empty plus CAR_{hCD19}, Empty plus CAR_{B7H3}, IFN plus CAR_{hCD19}, and IFN plus CAR_{B7H3} groups, respectively; survival model with random effects on experiment ID and administration route, see Materials and Methods). (**F** to **J**) Data from mice receiving CAR T cells by intravenous injection. (F) Absolute counts of CAR T cells in the PB 1 week after adoptive cell transfer. (G) Expression of the indicated markers on circulating $CD8^+$ CAR T cells by flow cytometry [diameter = % of positive cells; color code = MFI (median fluorescent intensity) of positive fraction; median values are plotted]. (H) Percentage of CAR T cells within the total T cell infiltrate in the tumor 22 days after adoptive cell transfer (Kruskal-Wallis tests with post hoc Dunn's correction). (I) Expression of the indicated markers on tumor-infiltrating $CD8^+$ CAR_{B7H3} T cells in Empty and IFN mice by flow cytometry [as in (H)]. (J) Percentage of tumor-infiltrating $CD8^+$ CAR_{B7H3} T cells highly coexpressing PD-1 and LAG-3 (defined as cells having fluorescence intensity above the third quartile of MFI distribution in all mice; Mann-Whitney U test). (**K**) Experimental outline of inducible IFN-α delivery by TEMs (ddIFN, destabilizing domain-fused IFN) and CAR T cells (see Supplementary Materials and Methods; TMP, trimethoprim; DHFR, dihydrofolate reductase). (**L**) Kaplan-Meier survival curves of n = 9 Empty plus CAR_{hCD19} mice, n = 10 Empty plus CAR_{B7H3} mice, n = 9 ddIFN plus CAR_{hCD19} mice, and n = 9 ddIFN plus CAR_{B7H3} mice (log-rank Mantel-Cox test with Bonferroni's correction). *P < 0.05, ***P < 0.001, and ****P < 0.0001.

Therapeutic efficacy was also observed with the combination of CAR_{B7H3} T cells and the inducible version of the TEM–IFN-α platform that we previously described (*7*), in which induction of IFN-α expression was performed after tumor establishment, thus better modeling a therapeutic strategy (Fig. 1, K and L).

To investigate whether similar therapeutic efficacy could be achieved by engineering IFN-α release from CAR T cells themselves, thus bypassing the need for HSC manipulation, we generated IFN-α–armored CAR T cells by means of BdLV coexpressing IFN-α and CAR. We produced IFN-α–armored CAR_{hCD19} and CAR_{B7H3} T cells to compare their therapeutic potential with that of their unarmored counterparts (fig. S5, A and B). Phenotypic characterization before infusion highlighted a modest skewing toward effector features induced by constitutive IFN-α armoring, without significant differences in the expression of ICRs (fig. S5, C and D). Intratumoral delivery of IFN-α–armored CAR_{B7H3} T cells in GBM-challenged wt mice did not elicit detectable toxicity but failed to achieve therapeutic efficacy that remained comparable to controls in terms of both tumor growth and mouse survival (fig. S5, E to G). Overall, these data showed that targeted IFN-α delivery by TEMs, but not by CAR T cells, could lead to robust CAR_{B7H3} T cell activity associated with increased expression of effector markers and decreased expression of ICRs.

Targeted delivery of orthogonal IL-2 safely improves CAR T cell function establishing a private cross-talk within the TME

We hypothesized that this platform could also deliver other cytokine payloads that may further boost CAR T cell proliferation and activity, such as interleukin-2 (IL-2). IL-2 can provide proliferative, survival, and activation support to effector T cells but can also favor T regulatory differentiation, which is detrimental for antitumor responses. To overcome this hurdle, IL-2 muteins able to preferentially bind a cognate IL-2Rβ mutein rather than the wt form, and thus target an engineered subset of T cells, have been recently described (*18*). These orthogonally acting pairs [ortho–IL-2 (oIL2) and ortho-IL2Rβ (oR)] effectively potentiated oR-bearing adoptive T cells in both syngeneic and xenogeneic tumor models by systemic administration of oIL2 (*18*–*20*). Although this strategy limits exposure of endogenous T cells to IL-2, thus mitigating counter-regulatory mechanisms and toxicities expected with the wt cytokine, systemic delivery of oIL2 was associated with weight loss and other adverse effects leading to death at the highest doses (*18*–*20*). Therefore, we reasoned that tumor-targeted TEM-mediated delivery could introduce a further level of control to this system and safely potentiate CAR T cell function against GBM.

We generated BdLV encoding for either CAR_{B7H3} or control CAR_{hCD19} coupled with oR ($oCAR_{B7H3}$ or $oCAR_{hCD19}$) (Fig. 2A). $oCAR_{B7H3}$ T cells were activated, released IFN-γ, and proliferated when cultured with target cells expressing B7-H3 in the presence of oIL2 variants, more robustly with $oIL2^{1G12}$ and more selectively with $oIL2^{3A10}$, consistent with their published properties (*18*) (fig. S6, A to D).

We then generated *Tie2-oIL2-miRT* LV for TEM-mediated delivery of $oIL2^{1G12}$ in the tumor (Fig. 2, A and B). HSCs transduced with either Empty or oIL2 LVs similarly engrafted in lethally irradiated recipient mice (fig. S7, A and B). Multilineage hemopoietic reconstitution was not affected by oIL2 gene therapy (fig. S7, C to J), although the cytokine was detected in the plasma at concentrations slightly higher than previously observed for IFN-α in our platform (*3*, *6*–*8*), possibly because of limited peripheral uptake by endogenous IL-2Rs (fig. S7K). Integrated LV was detectable in circulating nucleated cells at a median of 1.9 copies per genome (fig. S7L). In addition to the lack of signs of hemopoietic toxicities, there were no differences in body weights of oIL2 mice compared to those of Empty mice (fig. S7M).

After orthotopic tumor challenge, intratumoral injection of CAR_{B7H3} T cells with or without oR ($oCAR_{B7H3}$ and CAR_{B7H3}, respectively) was performed (Fig. 2B). Although no differences in tumor burden were detected at an early assessment (29 days after GBM injection), oIL2 mice that received $oCAR_{B7H3}$ T cells had almost stable lesions at later evaluation (44 days after GBM injection) (fig. S8A) and showed inhibition of tumor growth compared with Empty mice, with a trend toward maintaining a lower median tumor burden compared with oIL2 mice receiving CAR_{B7H3}T cells without the oR, although this did not achieve significance (Fig. 2C). oIL2 plus $oCAR_{B7H3}$ mice achieved a prolonged survival compared with all other groups (Fig. 2D). A slight reduction in tumor burden and trend toward improvement in survival, although not significant, were observed in oIL2 plus CAR_{B7H3} mice, in line with residual activity of oIL2 on the endogenous receptor.

In another set of experiments, Empty and oIL2 mice received either $oCAR_{B7H3}$ or $oCAR_{hCD19}$ T cells intratumorally (Fig. 2E). Significant reduction in tumor burden was observed only in oIL2-plus-$oCAR_{B7H3}$–treated mice (fig. S8B, $P = 0.0035$), without any apparent sign of toxicity such as significant weight loss (Fig. 2F). Higher abundance of oR-bearing adoptive T cells was observed in the tumor immune infiltrate of oIL2 mice compared with Empty mice (Fig. 2G and fig. S8, C to E), mainly of the $CD8^+$ subset (fig. S8C). GZMB had higher expression in $CD8^+$ and $CD4^+$ oCAR T cells of oIL2 mice compared with those of Empty mice (Fig. 2, H and I, fig. S8, F and G). However, only $oCAR_{B7H3}$ $CD8^+$ T cells increased the $PD\text{-}1^+LAG\text{-}3^+$ fraction in oIL2 mice (Fig. 2J), possibly because a more effective target-dependent activation under oIL2 stimulation may eventually drive exhaustion. Supporting the preferential binding of oIL2 to the oR, endogenous T cells were not affected in terms of abundance (Fig. 2K), $CD4^+/CD8^+$ composition (fig. S8D), and T regulatory differentiation (Fig. 2L) in any treatment group. Also in this setting, no B7-H3 antigen escape was detected (Fig. 2M).

Despite enhancing CAR-T activity, implementation of the oIL2-oR axis by TEM-based gene delivery provided an inferior therapeutic benefit than observed with IFN-α delivery. In a side-by-side comparison of the two platforms in combination with $oCAR_{B7H3}$ T cells, tumor growth was similarly delayed by the two treatments, but survival was more prolonged with IFN-α (HR = 0.26 and HR = 0.40 versus Empty mice, respectively) (Fig. 2, N to P). Because oIL2 and IFN-α are likely to act on different molecular pathways to enhance CAR T cell activity, we next assessed the efficacy and phenotypic impact on CAR_{B7H3} T cells of both cytokines and their combination.

Codelivery of IFN-α and oIL-2 potentiates CAR T cell rescue by promoting effector function and recruiting endogenous T cells against GBM antigens

We generated a *Tie2-Ifna1-P2A-oIL2-miRT* LV by inserting a self-cleaving P2A peptide coding sequence between the IFN-α and oIL2 ones (fig. S9, A to M). This construct enabled secretion of both cytokines by TIE2-expressing cells as observed in vitro and upon transplantation of engineered HSCs, even at lower extents compared with the respective monocistronic constructs at matched vector

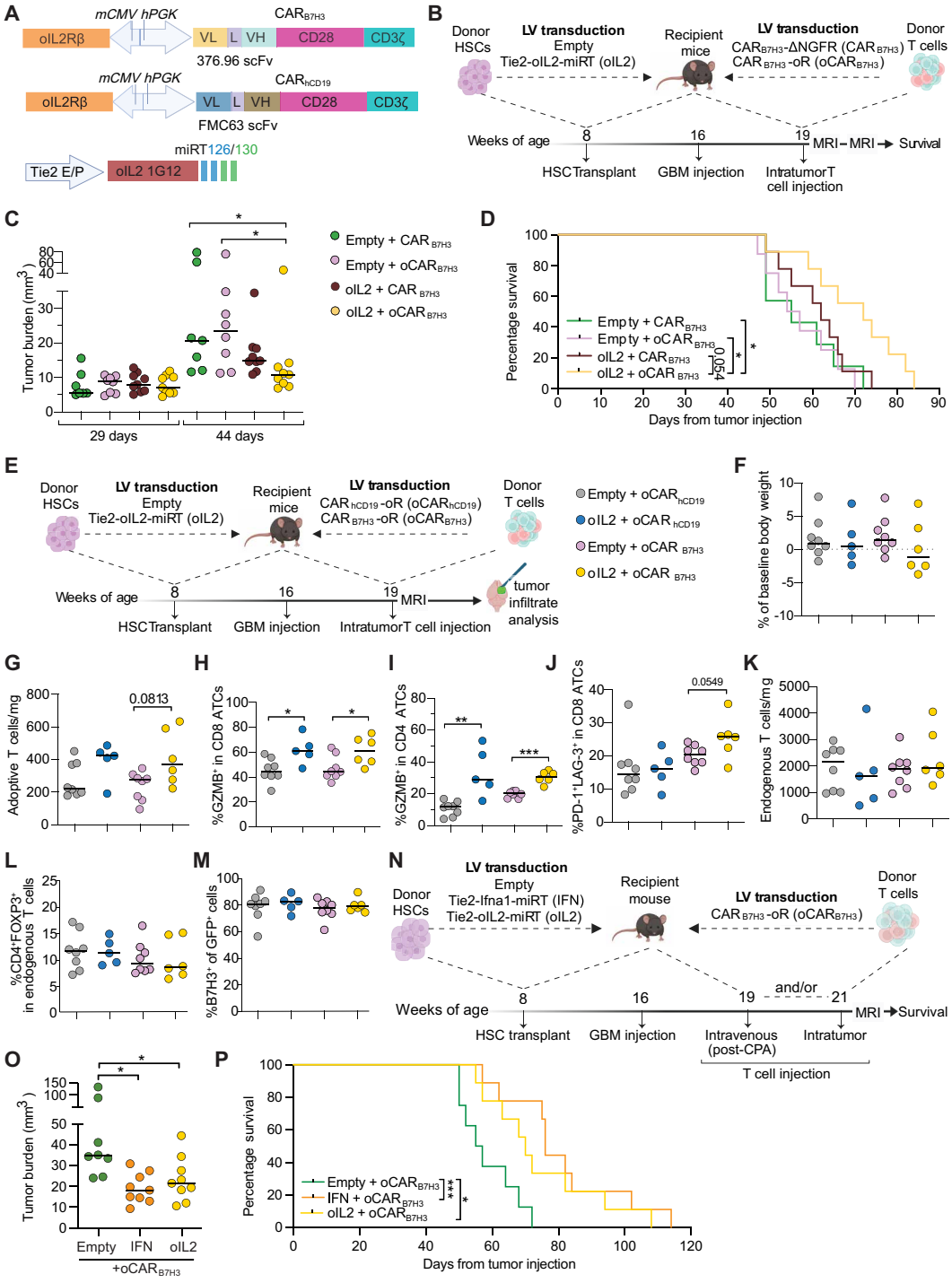

Fig. 2. The private cross-talk by the orthogonal IL-2/receptor pair via TEMs potentiates CAR T cells without perturbing endogenous T cells. (**A**) Schematic representation of oR-CAR$_{B7H3}$ BdLV, oR-CAR$_{hCD19}$ BdLV, and Tie2-oIL2-miRT LV. (**B**) Experimental outline for treatment efficacy evaluation: HSCs from donor mice were transduced with an empty (Empty) or Tie2-oIL2-mirT LV vector (oIL2) and transplanted into lethally irradiated C57BL/6 mice. After hematopoietic reconstitution, mGB2 cells were injected in the brain striatum. Mice received CAR$_{B7H3}$ T cells either expressing oIL2Rβ or not intratumorally. Tumor growth was monitored by MRI and survival analysis performed (n = 7 Empty plus CAR$_{B7H3}$, n = 8 Empty plus oCAR$_{B7H3}$, n = 9 oIL2 plus CAR$_{B7H3}$, and n = 9 oIL2 plus oCAR$_{B7H3}$). (**C**) Tumor burden evaluated by MRI 29 and 44 days after GBM injection in Empty and oIL2 mice (LME model, see Materials and Methods). (**D**) Kaplan-Meier survival curves of the four experimental groups of mice (log-rank Mantel-Cox test with Bonferroni's correction). (**E**) Experimental outline for tumor infiltrate analyses: HSC transduction and transplant and mGB2 injection were performed as in (B). Mice received oIL2Rβ-expressing CAR$_{B7H3}$ or CAR$_{hCD19}$ T cells intratumorally. Tumor growth was monitored by MRI, and immunophenotype characterization of tumor infiltrate was performed (n = 8 Empty plus oCAR$_{hCD19}$, n = 8 Empty plus oCAR$_{B7H3}$, n = 5 oIL2 plus oCAR$_{hCD19}$, and n = 6 oIL2 plus oCAR$_{B7H3}$). (**F**) Mouse weight changes (% of baseline) measured 40 days after tumor challenge. (**G** to **L**) Tumor infiltrate analyses performed 14 days after intratumor T cell injection. (G) Counts of adoptive T cells normalized on tumor weights. [(H) and (I)] Percentage of GZMB-expressing CD8$^+$ (H) and CD4$^+$ (I) adoptive T cells (ATCs). (J) Percentage of PD-1/LAG-3–coexpressing CD8$^+$ ATCs. (K) Counts of endogenous T cells normalized on tumor weights. (L) Percentage of CD4$^+$FOXP3$^+$ endogenous T cells. (**M**) Percentage of B7-H3 expression on tumor cells (GFP$^+$). [(F) to (M)] Kruskal-Wallis test with post hoc Dunn's comparisons. (**N**) Experimental outline for oIL2 and IFN gene therapy comparison in combination with CAR T cells: HSCs were transduced with Empty, oIL2, or IFN LVs, transplanted, and mGB2 injected as in (B). Systemic and intratumoral ACT was performed with oCAR$_{B7H3}$ in all mice (n = 8 Empty, n = 9 oIL2, and n = 9 IFN). Tumor growth was assessed by MRI, and survival analysis was performed. (**O**) Tumor burden evaluation by MRI 45 days after GBM injection. Kruskal-Wallis test with Dunn's post hoc analysis. (**P**) Kaplan-Meier survival curves for the different experimental groups (log-rank Mantel-Cox test with Bonferroni's correction). *P < 0.05, **P < 0.01, and ***P < 0.001.

copy numbers (Fig. 3A and fig. S9, B to D). Alternatively, cytokine codelivery by TEMs was achieved by transplanting mice with a mix of HSCs transduced with either *Tie2-Ifna1-miRT* or *Tie2-oIL2-miRT* LVs. Engraftment of engineered HSCs, hematopoietic reconstitution, and cytokine output in the peripheral blood were similar for the two codelivery strategies (fig. S9, E to K). IFN-α concentrations were higher in the tumor tissues of IFN and IFN plus oIL2 mice compared with the respective contralateral hemisphere (HB, healthy brain) and with tumors of Empty and oIL2 mice (fig. S9L), supporting tumor-specific cytokine release by engineered TEMs. We could not specifically measure the release of orthogonal IL-2 given the abundance of wt IL-2 released by recently injected CAR T cells that would have overwhelmed the former in an IL-2 detection assay. When combined with double route-administered $oCAR_{B7H3}$ T cells, both oIL2 and IFN-α, either alone or in combination, significantly inhibited tumor growth as compared with Empty mice (Fig. 3B, all $P < 0.05$). Codelivery of IFN-α and oIL2 by TEMs achieved a prolonged median overall survival (76 days) compared with either single treatment (oIL2: 59 days; IFN: 65 days) and Empty mice (56 days), corresponding to a substantial reduction in the risk of death by 91% (HR = 0.09) (Fig. 3C).

We next investigated T cell dynamics across the organism in these mice. We profiled tumor lesions; tumor-draining deep cervical lymph nodes (tdLNs); superficial cervical lymph nodes [non–tumor draining LNs (ntdLNs)]; and spleen, BM, and peripheral blood samples by a high-dimensional flow cytometry panel encompassing markers of T cell memory and effector differentiation, activation, exhaustion, and regulatory T cell (T_{reg} cell) markers (table S1). CD45-mismatched adoptively transferred and endogenous $CD3^+$ cells were separately analyzed by PhenoGraph (*21*), an algorithm capable of clustering single cells according to their relative expression of antigens. We identified 11 adoptive and 14 endogenous T cell PhenoGraph clusters, which showed a distinct tissue-specific distribution (Fig. 3, D and E, and fig. S10, A and B). Tumor-infiltrating adoptive T cells were characterized by high expression of the proliferation marker Ki-67, the activation/exhaustion marker PD-1, and the activation/tissue residency marker CD69 (Fig. 4A), whereas only a fraction of them expressed transcription factor 7 (TCF-7), a T cell memory marker related to tumor egression, which was instead more expressed in peripheral blood and LNs. These cells were mainly composed of $CD8^+$ clusters, among which cluster 4 was highly enriched by IFN-α and oIL2 and further by their codelivery (Figs. 3D and 4, A and B, and fig. S10C). These enriched cells expressed eomesodermin (EOMES) and T-box expressed in T cells (T-bet), known transcription factors (TFs) required by T cells to differentiate into effector phenotype; the activation marker CD25; and highly PD-1, likely representing CAR T cells robustly activated within the TME (Fig. 4A). Consistently, a CAR T cell subset characterized by high PD-1 expression was shown in previous studies to display superior cytotoxic function and persistence in the tumor site (*22*). Conversely, cluster 6, which was also found in tdLNs, was depleted upon cytokine delivery, especially in the combination group (Fig. 4B and fig. S10C). These cells expressed low amounts of activation markers (CD39, PD-1, and Ki-67) and high expression of TCF-7, representing a more stem-like population, possibly of nontransduced adoptive T cells (Fig. 4A). Altogether, these changes in cluster composition suggest a tumor-specific enrichment of activated CAR T cells by both cytokines without detectable off-target activation in the other tissues analyzed.

Endogenous tumor-infiltrating T cells were instead composed of a majority of $CD4^+$ cells (Fig. 3E). Cluster 5, the only $CD4^+$ GBM cluster highly expressing CD39, a marker associated with tumor reactivity (*23*) and effector markers (T-bet and CD44), was significantly increased in IFN and IFN plus oIL2 mice (both $P = 0.0024$, Fig. 4, C and D, and fig. S10D). Cluster 12, which was the only $CD8^+$ cluster identified in the tumor tissue, was similarly enriched in IFN and IFN plus oIL2 mice and showed expression markers of effector T cells (Fig. 4, C and D). In contrast, the more stem-like cluster 4, characterized by the absence of CD39 and higher expression of TCF-7, was underrepresented in tumors of IFN and IFN plus oIL2 mice and likely represented bystander cells (Fig. 4, C and D). $CD39^+$ putative tumor-reactive endogenous $CD8^+$ cells could also be identified in the peripheral blood, BM, and spleen [cluster 10 of more naïve and cluster 14 of short-lived effector killer cell lectin-like receptor G1 ($KLRG\text{-}1^+$) cells] and were significantly increased by IFN and IFN plus oIL2 (all $P \leq 0.0144$, Fig. 4, C and D, and fig. S10D). Last, the central-memory cluster 7, coexpressing EOMES and TCF-7, was increased in the peripheral blood and LNs of IFN and IFN plus oIL2 mice. Altogether, these changes in endogenous T cell clusters suggested the engagement of a systemic antitumor response specifically triggered in the presence of IFN-α. Conversely, the lack of major phenotypic changes in the endogenous compartment of oIL2 mice supported the private cross-talk established between TEMs and $oCAR_{B7H3}$ T cells selectively in the GBM TME.

To functionally validate the findings of boosted effector function of $oCAR_{B7H3}$ T cells and endogenous T cells by cytokine treatments, we performed IFN-γ ELISPOT with peripheral blood mononuclear cells (PBMCs) and tumor-infiltrating lymphocytes (TILs) on B7-H3–positive or –negative mGB2 cells (Fig. 4, E and F). T cells in peripheral blood reacting to mGB2 by targeting B7-H3 increased with IFN-α gene therapy and further by the codelivery of the two cytokines, despite the frequency of adoptively transferred cells being similar across all conditions (fig. S9M). Functional analysis of TILs highlighted similarly increased proportions of B7-H3–reactive cells in IFN and IFN plus oIL2 mice compared with oIL2 and Empty mice. The lack of a significant effect of oIL2 alone on the proportion of B7-H3–reactive T cells in this functional assay may suggest dysfunctional activation of CAR T cells in the absence of concurrent IFN-α stimulation. T cells reacting against $B7\text{-}H3^-$ mGB2 cells also increased with IFN-α and further with its combination with oIL2, both in peripheral blood and in tumor infiltrates, suggesting a pivotal role of IFN-α in triggering antigenic spreading and priming of endogenous T cells, which could be further promoted by concomitant orthogonal stimulation of oCAR T cells by oIL2. In line with this contention, IFN plus oIL2 mice receiving $oCAR_{B7H3}$ T cells showed similar survival if challenged with tumor cells expressing B7-H3 in all or only a fraction (50%) of them and significantly longer than $oCAR_{B7H3}$ T cell–treated Empty mice ($P = 0.0045$ and $P = 0.0011$, respectively), supporting the engagement of endogenous T cells in mediating, at least in part, the improved antitumor activity of the combination strategy (Fig. 4, G and H).

CAR T cells maintain transcriptional features of functional effector cells upon cytokine delivery into the TME

To investigate the impact of the different cytokine deliveries on CAR T cell fate in the TME at the transcriptional level, we performed a single-cell RNA sequencing (scRNA-seq) analysis of sorted adoptive

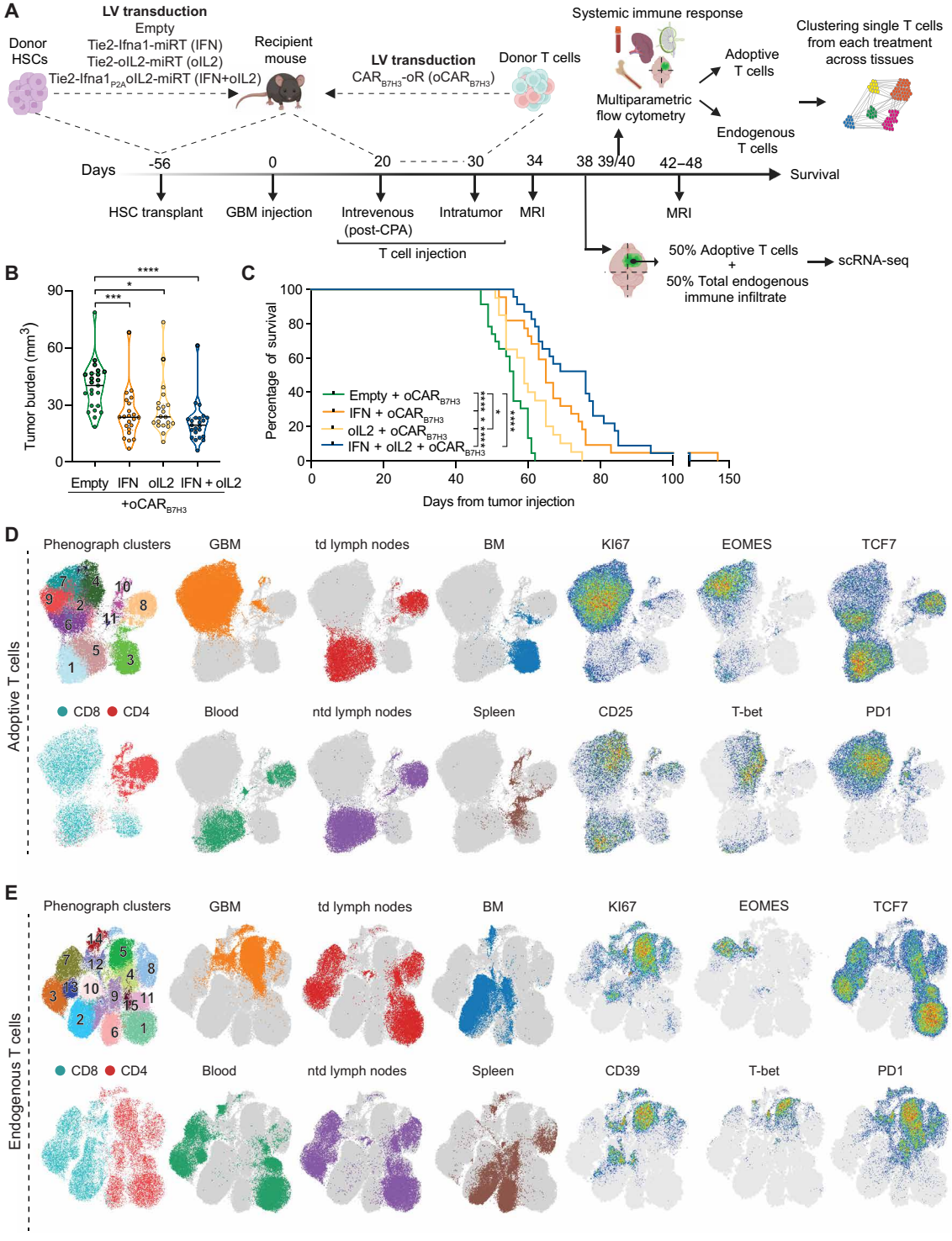

Fig. 3. Codelivery of tumor-targeted IFN-α and oIL2 potentiates CAR T cells and improves therapeutic efficacy. (**A**) Experimental outline: HSC transplantation, GBM injection, and ACT were performed as in Fig. 2N with the addition of a group of mice engineered to codeliver IFN and oIL2 at the tumor site. Survival analysis, immunophenotypic characterization, and single-cell RNA sequencing (scRNA-seq) were performed as depicted and described in Supplementary Materials and Methods. Tumor growth was monitored by MRI performed 42 to 48 days after GBM injection in survival studies or 34 days after GBM injection in experiments involving tissue analysis. (**B**) Tumor burden assessment by MRI 42 to 48 days after GBM injection ($n = 3$ independent experiments; $n = 23$, 22, 20, and 23 mice in Empty plus oCAR$_{B7H3}$, IFN plus oCAR$_{B7H3}$, oIL2 plus oCAR$_{B7H3}$, and IFN plus oIL2 and oCAR$_{B7H3}$ groups, respectively; LME with random effects on experiment ID, see Materials and Methods). (**C**) Kaplan-Meier survival curves of mGB2-bearing mice from different treatment groups [$n = 3$ independent experiments, as in (B); survival model with random effects on experiment ID, see Materials and Methods]. (**D** and **E**) Left: uniform manifold approximation and projection (UMAP) analysis of concatenated live CD3$^+$ adoptively transferred (D) and endogenous (E) PhenoGraph clusters from tumor lesions ($n = 5$, orange); tdLNs ($n = 2$, red); ntdLNs ($n = 5$, purple); and PB ($n = 5$, green), BM ($n = 5$, blue), and spleen ($n = 5$, brown) samples. Both global dataset and tissue distribution are reported. CD4/CD8 positivity of cells is depicted at the bottom left. Right: UMAP plot showing distribution of positive cells for selected markers throughout the global dataset. *$P < 0.05$, ***$P < 0.001$, and ****$P < 0.0001$.

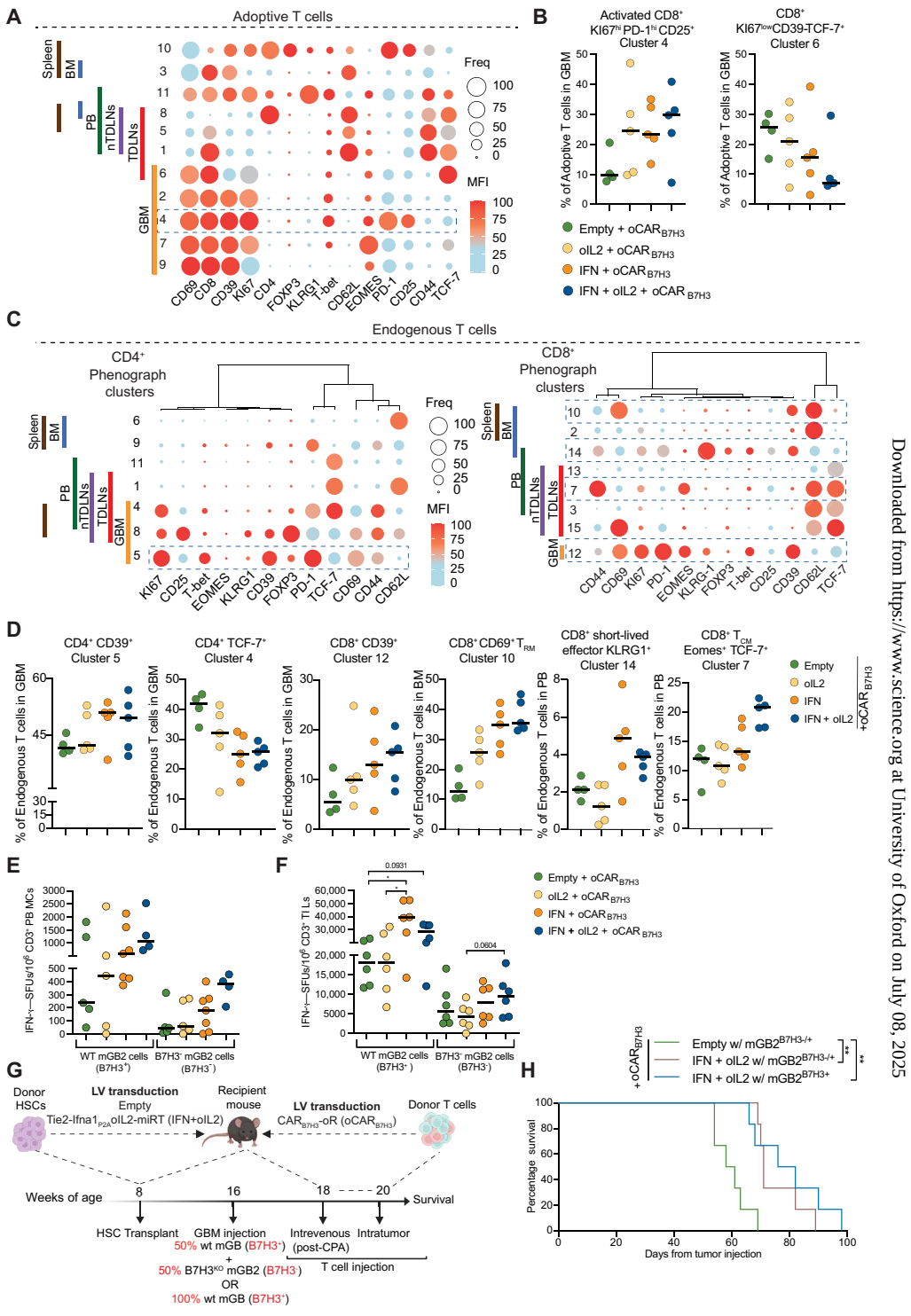

Fig. 4. Rewiring of adoptive and endogenous T cells upon targeted cytokine delivery promotes antitumor effector function. (**A**) Balloon plots showing the expression (frequency, Freq) and the MFI of specific markers (columns) in discrete PhenoGraph clusters (rows) of adoptively transferred T cells from multiple tissues as indicated in Fig. 3 (A and D). Unbiased hierarchical meta clustering grouped markers with similar immune phenotypes. (**B**) PhenoGraph cluster frequencies (%) of adoptive T cells across treatments in specified tissues. Each dot represents a mouse ($n = 4$ Empty, $n = 5$ IFN, $n = 5$ oIL2, and $n = 5$ IFN plus oIL2). (**C**) Balloon plots showing the expression (frequency, Freq) and the MFI of specific markers (columns) in discrete PhenoGraph clusters (rows) of endogenous T cells from multiple tissues as indicated in Fig. 3 (A and E). Unbiased hierarchical meta clustering grouped markers with similar immune phenotypes. (**D**) PhenoGraph cluster frequencies (%) of endogenous T cells across treatments in specified tissues. Each dot represents a mouse ($n = 4$ Empty, $n = 5$ IFN, $n = 5$ oIL2, and $n = 5$ IFN plus oIL2). (**E** and **F**) IFN-γ spot forming unit (SFU) per million of $CD3^+$ PBMCs (E) from $n = 5$ Empty, $n = 7$ IFN, $n = 5$ oIL2, and $n = 4$ IFN plus oIL2 mice and $CD3^+$ TILs (F) from another cohort of $n = 6$ Empty, $n = 6$ IFN, $n = 6$ oIL2, and $n = 6$ IFN plus oIL2 mice cultured on either wt or $B7\text{-}H3^-$ mGB2 cells as feeders. The assays were performed after 14 and 3 days from intravenous and intratumor adoptive T cell transfer, respectively [Kruskal-Wallis test with post hoc comparisons with Dunn's correction performed only in (F) because the experimental groups had $n \geq 5$ replicates]. (**G**) Experimental outline to assess impact of target antigen heterogeneity on treatment efficacy. Mice were transplanted with Empty- or Tie2-Ifna1-P2A-oIL2-mirT LVs (IFN plus oIL2). Tumor challenge was performed with 100% wt mGB2 cells ($B7H3^+$) or a 1:1 mix of wt and $B7H3^{KO}$ cells (see Supplementary Materials and Methods). Systemic and intratumoral ACT was performed with $oCAR_{B7H3}$ in all mice. (**H**) Kaplan-Meier survival curves of $oCAR_{B7H3}$ T cell–treated Empty ($n = 6$) and IFN plus oIL2 ($n = 6$) mice challenged with mixed $B7H3^+/B7H3^-$ mGB2 cells and IFN plus oIL2 mice ($n = 6$) challenged with wt $B7H3^+$ mGB2 cells (log-rank Mantel-Cox test with Bonferroni's correction). $^*P < 0.05$ and $^{**}P < 0.01$.

and endogenous $CD45^+$ tumor-infiltrating cells admixed at a 1:1 ratio (Figs. 3A and 5A and fig. S11A). After unsupervised clustering (table S2), we mapped the woodchuck hepatitis virus posttranscriptional regulatory element (*WPRE*) sequence downstream of the *CAR* transcript to identify transduced cells and then focused the analysis on the *Cd8*-expressing CAR T cells (Fig. 5A and fig. S11B). Concerning the myeloid cell populations of the TME, we identified 13 unsupervised clusters, which were annotated according to lineage markers. Among them, we identified three TAM clusters characterized by the well-described marker genes *C-X-C motif chemokine 9* (*Cxcl9*) (*24*), *interleukin 1 beta* (*Il1b*) (*25*), and *secreted phosphoprotein 1* (*Spp1*) (*24*) and four dendritic cell (DC) clusters, comprising conventional DC1s (cDC1s), cDC2s, plasmacytoid DCs (pDCs), and DCs enriched in immunoregulatory molecules (mregDCs)

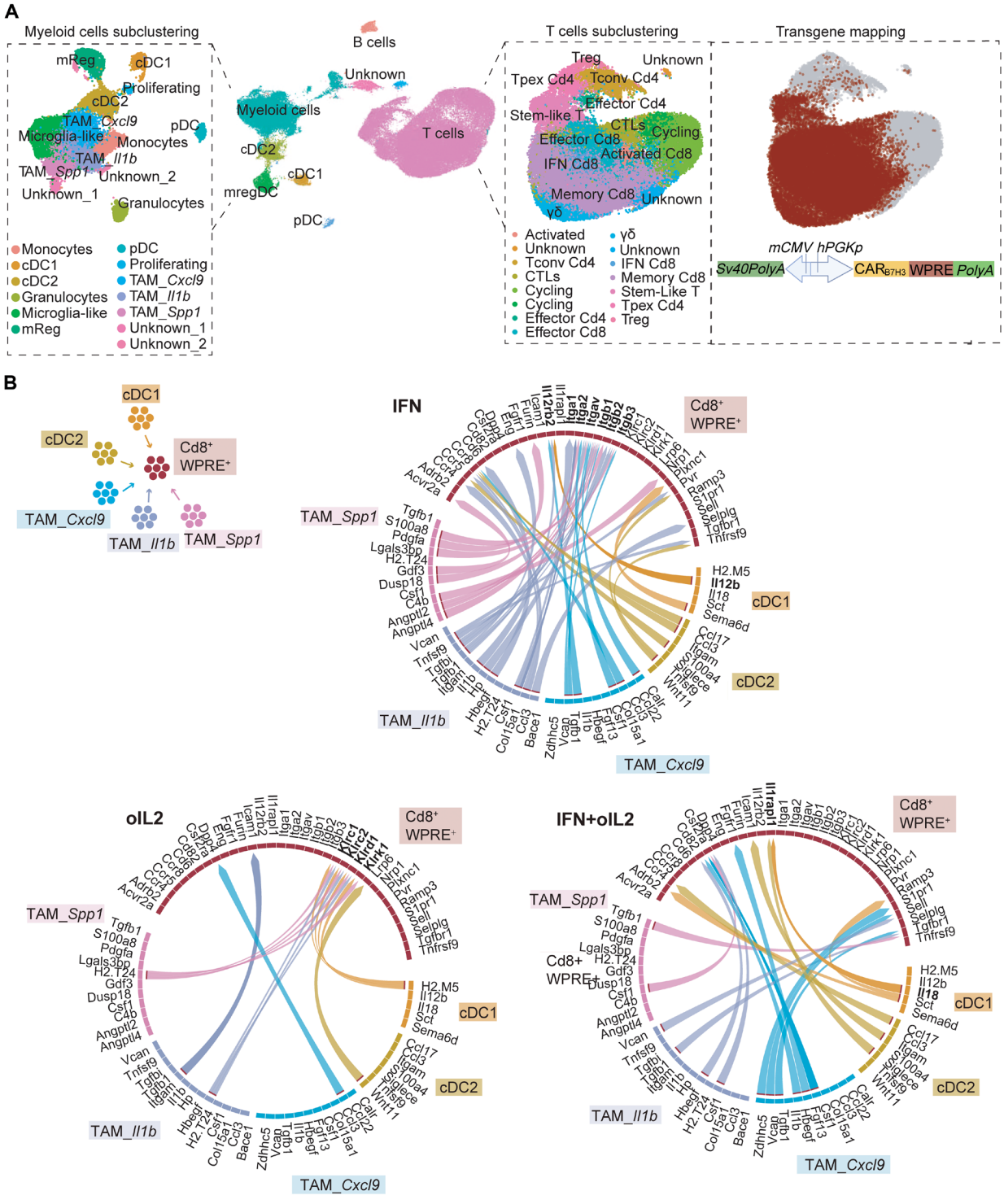

Fig. 5. scRNA-seq analyses of immune infiltrating cells highlight differential communication patterns between CAR T cells and myeloid cells in response to targeted cytokine delivery. Mice were treated as depicted in Fig. 3A and euthanized 38 days after tumor injection, and then GBMs were isolated and dissociated ($n = 3$ per group). Endogenous and adoptive immune cells were separately sorted on the basis of CD45 mismatch, and scRNA-seq was performed using Chromium Controller (10X Genomics) by mixing 1:1 adoptive and endogenous cells from each mouse. (**A**) Middle: UMAP plot representing GBM-infiltrating immune cells of the entire dataset colored by cell type ($n = 73{,}812$) obtained by merging all of the samples and applying fastMNN batch correction. Clusters were obtained with Louvain unsupervised clustering at a resolution of 0.6. Left: UMAP of myeloid cells colored by clusters ($n = 20{,}478$). Right: UMAP of T cells colored by cluster ($n = 48{,}914$) and in silico sorted Cd8$^+$ and WPRE$^+$ T cells ($n = 28{,}234$). (**B**) Chord diagram visualization of the top 75 prioritized interactions between TAMs/DCs and CAR T cells using MultiNicheNet (see Supplementary Materials and Methods). Arrows indicate the directions from sender to receiver cell type. Colors indicate the sender cell type expressing the ligand. Each interaction is assigned to the treatment group that up-regulates it most when compared with control.

(Fig. 5A and table S2). We then performed an analysis of the intercellular communications that may bridge innate and CAR T cell immune responses using multiNicheNet (*26*), a method that predicts ligand-target links between interacting cells by combining their expression data with prior knowledge of signaling and gene regulatory networks (Fig. 5B). Specifically, we analyzed cell-to-cell communication between TAMs and conventional DCs toward *Cd8*-expressing CAR T cells, comparing each treatment group against Empty controls. The 75 top-ranked up-regulated ligand/receptor pairs (table S3) were univocally assigned to the treatment that displayed the strongest expression in the sender cells and whose predicted target genes were enriched in receiver cells compared with the other treatments. Whereas IFN treatment induced broad cross-talk between different myeloid cell types and CAR T cells over control, highlighting substantial reshaping of the TME by this pleiotropic cytokine, oIL2 showed limited changes, consistent with the private features of the established orthogonal circuit. Top predicted IFN-α–specific ligands included cDC1-sourced *Il12b*, potentially able to generate effector IL12Rβ$^+$ CAR T cell progeny (*27*), as well as TAM-sourced ligands for a variety of integrins (*Itga2, Itgb1, Itgb2*, and *Itgav*), some of which have been associated with cytotoxic T cells (*28*). When comparing TAM–CAR T cell cross-talk between IFN alone and combined with oIL2, we noted a skewing from immunosuppressive *Spp1*$^+$ TAMs to inflammatory *Cxcl9*$^+$ TAMs on the sender side, suggesting an interaction more tuned to T cell activation. However, *Tgfb-Tgfbr1* interaction emerged between *Spp1*$^+$ TAMs and CAR T cells in the combination group, possibly representing a negative feedback loop toward the treatment-dependent enrichment of activated T cells in the TME. Nevertheless, CD28-costimulatory domain-bearing second-generation CAR T cells have been described to be, at least partially, resistant to TGF-β–mediated repression of T cell proliferation (*29*). Moreover, in IFN plus oIL2 mice, the analysis highlighted a cDC1–CAR T cell *Il18-Il1rapl1* interaction, which may expand effectors without eroding the memory pool in the TME (*30*). Conversely, the strongest oIL2-specific interactions between myeloid and CAR T cells involved several major histocompatibility complex (MHC) and KLRG molecules, revealing the occurrence of possible CAR T cell dysfunction on the basis of T cell–to–NK cell transition related to continued exposure to antigen stimulation (*31*).

Overall, these analyses suggested that IFN-α signaling, especially when combined with oIL2, induces a multifaceted intercellular network in the TME that sustains a more activated CAR T cell state. To deepen the analysis on this state, we next projected the CAR T cell scRNA-seq data into a reference atlas of mouse TILs using ProjecTILs (*32*), which showed that almost half of CAR T cells in Empty mice mapped to a CD8$^+$ exhausted T cell subtype (Tex) (Fig. 6A), characterized by high expression of granzymes, multiple ICRs [*programmed cell death protein 1* (*Pdcd1*), *Ctla4*, *lymphocyte activation gene 3* (*Lag3*), and *T cell immunoreceptor with Ig and ITIM domains* (*Tigit*)], and *thymocyte selection–associated high mobility group box* (*Tox*) genes. This Tex fraction was markedly reduced upon cytokine delivery, in particular in IFN plus oIL2 mice, where they accounted for <25% of *Cd8*-expressing CAR T cells. Conversely, naïve-like cells increased upon all treatments, with oIL2 and IFN also showing a trend for increasing the early activated and effector/memory subtype, respectively, and their combination showing an additive effect (Fig. 6A). The same analyses were performed with *Cd8*-expressing CAR-negative cells, which may comprise both endogenous T cells as well as untransduced adoptively transferred cells. ProjectTILs revealed a substantial increase in the proportion of effector/memory cells upon cytokine delivery, which reached up to 60% with their combination, whereas individual cytokine treatments also showed an increase in the Tex fraction (Fig. 6A). Overall, these analyses suggested that targeted cytokine delivery reduced terminal exhaustion of CAR T cells in the TME and sustained an effector memory pool, with IFN-α providing the major contribution. We also observed a skewing toward an effector gene signature of *Cd4*$^+$ *WPRE*$^+$ cells in the presence of IFN, despite the low number of these CAR T cells among all conditions (fig. S12). Furthermore, these changes were accompanied by activation of CAR-negative TILs, conceivably against tumor antigens, that acquire the most functional, effector/memory transcriptional state upon combined delivery of oIL2 and IFN-α.

We further identified master transcriptional regulators that underlie CAR T cell transcriptional changes upon cytokine treatments by applying SCENIC (single-cell regulatory network inference and clustering), a computational pipeline able to predict TF activity (regulon activity) by the analysis of TF motifs that are enriched at the promoters of expressed genes in scRNA-seq data (*33*) (Fig. 6B and table S4). Among the top-ranking activated regulons in CAR T cells from IFN plus oIL2 mice, several were associated with effector memory states [*Fos, Fosb, Jun, nuclear factor kappa B subunit 1* (*Nfkb1*), and *signal transducer and activator of transcription 5a* (*Stat5a*)] (*34*, *35*) or interferon activation (*Stat1/Stat2*, Irf-family members). Of note, one of the latter, *Irf7*, was associated with superior tumoricidal capacity of CD28-based CAR T cells (*36*). Among the regulons more specifically activated upon IFN-α delivery were *forkhead box protein O1*, *Foxo1*, a TF known to preserve memory phenotype and enhance antitumor function and metabolic fitness in CAR T cells during chronic antigen stimulation (*37*); and *Foxp1*, associated with stem-like features (*38*). Conversely, oIL2 increased regulon activity of *negative elongation factor complex member E* (*Nelfe*), a subunit of Nelf, an RNA polymerase II pausing factor that is critical for T cell proliferation, persistence, and memory generation during antitumor response (*39*); as well as *zinc finger protein of the cerebellum 1* (*Zic1*), *Thanatos-associated protein 11* (*Thap11*), *zinc finger protein 454* (*Zfp454*), and *zinc finger and SCAN domain containing 29* (*Zscan29*), whose functions in T cell biology remain poorly characterized. Conversely, Empty mice were characterized by signs of dysfunction such as higher *Zfp143* regulon activity, associated with terminal exhaustion (*40*), and *basic leucine zipper ATF-like TF 3* (*Batf3*), related to dysfunctional hyperproliferation of CAR T cells (*41*). These findings further support a major cytokine-dependent reshaping of the CAR T cell population in the TME toward better preservation of functional states driven by the integrated activation of subtype-specific transcriptional regulatory networks.

Overall, the signaling axes and transcription activation networks enhanced by IFN-α, oIL2, or their combination in the TME provide mechanistic insight into the observed rescue of CAR T cell functionality, consistent with some previously reported molecular targets and uncovering some potentially actionable targets as well.

DISCUSSION

Here, we show that CAR T cells against the clinically relevant antigen B7-H3 are rescued in the hostile GBM TME by tumor-targeted cytokine delivery and can achieve therapeutic efficacy in

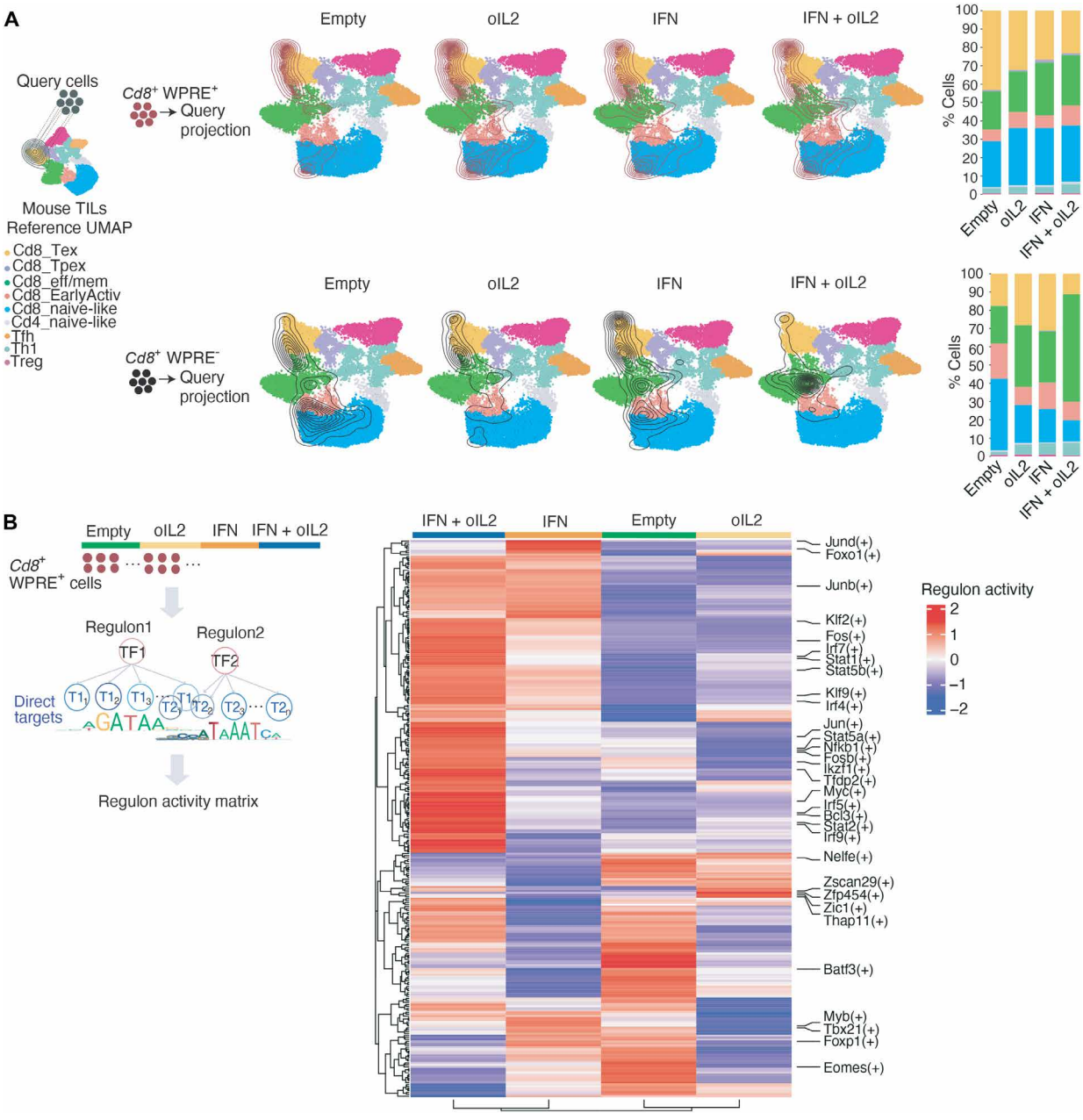

Fig. 6. Transcriptional landscape of tumor-infiltrating T cells upon cytokine delivery into the TME. (**A**) Left: UMAP plots showing the projections of Cd8$^+$/WPRE$^+$ and Cd8$^+$/WPRE$^-$ cells (query cells) into a reference TIL atlas. Reference atlas states are indicated as colored cells. Contour lines represent the density of projected query cells. Right: Bar graphs depicting the subtype composition for each treatment. (**B**) Left: SCENIC pipeline. Right: Heatmap of regulon activity in each treatment group. Relevant transcription factors, manually selected, are listed.

an immunocompetent GBM model that did not respond to CAR T cells alone. Locally released IFN-α prevented precocious terminal exhaustion of exogenously administered CAR T cells and enhanced the frequency and activation of their effector/effector memory phenotype, which is mainly responsible for tumor cell killing. Moreover, the combination of TEM-based IFN-α delivery and CAR T cells effectively engaged the endogenous T cell compartment toward broader tumor-specific reactivity beyond the CAR target, as shown by transcriptional profile, surface phenotype, functional assays, and the resistance to rechallenge with B7-H3–negative GBM cells by a mouse that cleared the primary tumor. Antigenic spreading is a highly sought-after and powerful means to establish durable antitumor protective immunity, and its induction here could be ascribed to the bridging functions between innate and adaptive immunity by IFN-α. Upon tumor cell killing induced by CAR T cells, macrophages, DCs, and other antigen-presenting cells, such as inflammatory monocytes (*42*), may uptake tumor-associated antigens and more effectively present them to endogenous T cells under IFN-α exposure, which allows up-regulation of MHC-I, MHC-II, and costimulatory molecules (*43*–*45*). As a result, the combination

approach provided tumor control and survival advantage not only over CAR T cells but also over IFN-α monotherapy. The same survival advantage was also observed with inducible TEM-based IFN-α delivery (*7*), actioned once tumors are already established, providing a more stringent validation of its translational potential.

Some reports have shown that T cell exposure to type I IFN can exert a detrimental impact and trigger an exhaustion program (*46*, *47*). These findings could be due to high and/or fluctuating systemic concentrations of type I IFN, whereas the gene therapy strategy described here accounts for low, stable, and sustained release of the cytokine preferentially at the tumor site. We have already demonstrated that systemic treatment with recombinant IFN-α failed to prolong GBM-bearing mouse survival, whereas gene therapy substantially extended it (*7*).

The implementation of the orthogonal IL-2/IL2Rβ axis by TEMs and CAR T cells allowed the establishment of a private cross-talk between the two engineered cell types specifically in the TME (*18*–*20*). TEM-mediated release of oIL2 in the tumor led to an increase in the intratumor abundance of oR-bearing CAR T cells and specifically promoted the early activation of $oCAR_{B7H3}$ T cells. However, unlike IFN-α gene therapy, this effector phenotype evolved in a dysfunctional state associated with a gene expression program linked to a T cell–to–NK cell–like transition (*31*). Recent evidence suggests that immunosuppressive molecules in the TME such as prostaglandin E2 impair IL-2 sensing of $CD8^+$ TILs by down-regulating the IL-2Rγ chain, resulting in the defective assembly of IL2Rβ-IL2Rγ and T cell dysfunction (*48*, *49*). Such impairment, if similarly occurring in murine T cells, may also affect our oIL2R reconstitution strategy, because we only delivered the IL2Rβ mutein and it can, conceivably, be overcome by the concurrent establishment of IFN-α signaling. On the other hand, oIL2 did not affect endogenous T cells, highlighting (i) the specificity and privateness of the cross-talk with TEMs, accounting for the safety of the approach, and (ii) the likely absence of immune response toward CAR-unrelated tumor-associated antigens without IFN-α delivery. Decreased tumor growth and improved survival were achieved with the orthogonal platform, but to a lower extent compared with IFN-α delivery. The dysfunctional transcriptional profile of CAR T cells supplied with exogenous oIL2 signaling was closer to that of control mice as compared with other treatments, further highlighting the need for a pleiotropic stimulatory cytokine, such as IFN-α, to overcome the immunosuppressive GBM TME. On the safety aspect, we exploited a more potent but less specific form of oIL2 (1G12) that improved the antitumor activity of CAR T cells without causing overt toxicity, which was previously observed upon systemic oIL2 administration in a dose-dependent fashion (*18*–*20*). In future studies, our platform could be endowed with other orthogonally acting cytokines, to selectively enhance tumor homing of CAR T cells from the periphery.

Codelivery of IFN-α and oIL2 by TEMs achieved further potentiation of $oCAR_{B7H3}$ T cells by preserving more effector and memory phenotypes and better preventing terminal exhaustion. Moreover, it effectively engaged the endogenous T cell compartment more extensively than delivery of IFN-α alone to establish a systemic immune response against tumor-associated antigens other than the CAR target, reflected in preserved survival advantage also in the case of the heterogeneous expression of the CAR target antigen by the tumor. The relevance of cytokine-promoted engagement of endogenous immunity and antigenic spreading to achieve sustained CAR T cell efficacy is in agreement with recent studies (*50*).

Codelivery of IFN-α and oIL2 induced a transcriptional skewing of CAR-negative TILs toward an effector memory state, which was not established in the presence of single cytokines. This could be due to the requirement for recognition of neo-epitopes in the presence of costimulatory signals, putatively achieved by oIL2-boosted tumor cell killing by CAR T cells in the presence of IFN-α. Despite the simultaneous presence of such immunostimulant cytokines, their spatial constraint in the tumor site avoided the onset of any overt toxicity that could have hampered clinical transability of the approach.

By using independent technologies to characterize CAR T cells under the different experimental conditions, we showed that IFN-α and oIL2 induce both specific and shared changes in CAR T cell cellular composition. A contraction of the terminally exhausted fractions and a concomitant enrichment of the stem-like fractions were observed with both treatments, whereas IFN-α specifically induced an effector memory state and oIL2 induced an early activated state. Their codelivery resulted in a bridging state between the two that was phenotypically reflected by a more robustly activated profile.

Among the limitations of the current study is the reliance on a single GBM experimental model, which includes the use of a specific CAR target, B7-H3, and a single costimulatory domain, CD28. However, available evidence indicates poor efficacy of 4-1BB–costimulated murine CAR T cells compared with the well-established functionality of their human counterparts (*51*–*53*). Nevertheless, we leveraged a hard-to-treat immunocompetent GBM model that better recapitulates several features of the human disease (*12*), including TEM recruitment, and abrogated the therapeutic efficacy of CAR T cells, as observed in clinical trials (*11*, *54*), making the efficacy improvements described here of translational relevance. Despite treatment delaying tumor growth and extending overall survival, residual tumor remained in most cases. Whether this reflects the rapid growth of orthotopic tumor models that outpace deployment of fully protective immune response or intrinsic challenges of this tumor type remains unknown. However, the continued progress in CAR molecular design promises enhanced functionality and could achieve greater therapeutic efficacy when implemented with our combination strategy. To this aim, the optimized manufacturing protocol for murine CAR T cells presented here could facilitate future testing of next-generation murine CAR T cells in syngeneic settings.

Another limitation of our study comes from the temporal window of phenotypic and transcriptomic characterization of CAR T cells after sequential systemic and loco-regional administration, which, although mimicking the latest clinical approach (*55*–*57*), fails to ascribe specific effects to either route. Whereas the closer time of analysis to the intratumor injection allowed capturing the evolving heterogeneity of CAR T cells within the TME, systemic characterization may have been limited to the few cells that persisted longer than short-lived effectors.

Different targeted cytokine delivery approaches have been tested in GBM models, including T cell armoring (*2*, *58*) and antibody-cytokine conjugates (*59*). Although these strategies offer selectivity compared with systemic cytokine administration, they introduce additional challenges, including the potential augmentation of CAR-related toxicities and the inability to rescue poorly functional CAR products. T cells may have limited persistence in the TME or, conversely, undergo unpredictable expansion and contraction phases, because of CAR tonic signaling and on- and off-tumor activation, hindering precise dosing of cytokine output. This can contribute to severe toxicity, as shown by IL-12–armored TILs and CAR T cells

inducing life-threatening hemophagocytic lymphohistiocytosis/macrophage activation-like syndrome in patients with metastatic melanoma (*60*) and ovarian cancer (*61*). Antibody conjugates may cause higher systemic exposure to the cytokine, a fluctuating kinetic and poor biodistribution within the tumor tissue. Compared with these strategies, the TEM platform provides a T cell–independent, sustained, and localized release of cytokines in the GBM TME, which is remodeled to promote a more activated and less suppressive milieu before adoptive T cell transfer. On the other hand, the TEM platform relies on autologous HSC engineering and transplantation, introducing further therapeutic complexity for fragile patients. Other approaches to local cytokine delivery independent from the T cells could include genetically engineered myeloid cells (*62*) and DCs (*63*).

In this study, IFN-α release by CAR T cells was not able to rescue therapeutic activity. This difference in efficacy from engineered TEMs may not be ascribed to different times of cytokine delivery in the tumor because we demonstrated comparable survival by inducing IFN-α release by TEMs when tumors were already established. Rather, exposure to IFN-α already during manufacturing and, conceivably, to higher in vivo concentrations than achieved by the TEM strategy may lead to dysfunctional T cell activation. Although more sophisticated engineering strategies, such as inducible release upon target recognition, may overcome this hurdle, the limitations imposed by T cell–based delivery mentioned above may remain unaddressed.

From a translational perspective, we have explored a combination strategy between two gene and cell therapies already undergoing clinical evaluation for patients with GBM (Temferon and multiple CAR T cell therapies, including B7-H3–targeting CARs sharing the same scFv as used in our mouse experiments). Interim data from the Temferon clinical trial (NCT03866109, Genenta Science) demonstrated the safety and tolerability of the approach with absence of dose-limiting toxicities and evidence of reprogramming of the TME (*64*). On the one hand, recent trials of CAR T cell therapies for GBM have highlighted the potential of these therapies to achieve prompt and robust responses in a fraction of patients, but, on the other hand, none have yet shown a sustained long-term benefit, and multiple resistance mechanisms exist that still need to be fully uncovered and overcome (*56*, *65*, *66*). It is conceivable that the combination approach explored here in the preclinical context may improve therapeutic benefits in patients. Furthermore, the broad expression of B7-H3 and the presence of TEMs in several tumor types suggest expansion of this combination strategy across multiple clinical indications.

MATERIALS AND METHODS

Study design

In the present study, we aimed to (i) demonstrate the rescue of CAR T cell efficacy in a hard-to-treat solid tumor model by tumor-targeted delivery of immune stimulating cytokines; (ii) establish a private cross-talk between TEMs and CAR T cells by implementing an orthogonal cytokine and receptor pair in the platform; and (iii) gather mechanistic characterization of the transcriptional and phenotypic changes accounting for therapeutic efficacy.

In vitro experiments were performed with at least five biological replicates of primary cells and/or cell lines to perform nonparametric statistical analyses (as specified in figure legends). In vivo experiments were performed with previously estimated numbers of mice by statistical analyses powered to highlight differences in efficacy and accounting for variability observed in previous experiments performed with the same GBM model. When analyzing multiple experiments with the same setting, linear mixed-effect (LME) and survival models accounted for experiment ID and, when specified, CAR T cell administration route as random effects. Some observations identified as outliers by the statistical models were excluded in an unsupervised manner (see the "Statistical analyses" section). All of the treatment groups included at least five experimental mice to perform nonparametric statistical analyses (as specified in figure legends). All continuous variables are graphically represented as median and individual data points.

When mice of the same treatment group received either CAR_{B7H3} T cells or CAR_{hCD19} T cells, randomization was performed to match vector copy number on nucleated peripheral blood cells and plasma cytokine concentration at the time of hematopoietic reconstitution in the two subgroups. Efficacy outcomes of different cytokine delivery were collected from $n \geq 3$ experiments. Specific procedures like scRNA-seq and multiparametric flow cytometry analyses were conducted only once and with $n \geq 3$ experimental mice because of the technical complexity.

Tumor burden measurement by MRI was performed by two independent unblinded operators. Graphical representation of experimental outlines and data was performed with Prism8, Adobe Illustrator, R-Studio, and Biorender (licensed for publication to Ospedale San Raffaele—SR-Tiget).

Mice

C57BL/6 mice, CD45.2 or CD45.1, were purchased from Charles River Laboratory. CD45.1/CD45.2 mice were obtained by the cross-breeding of CD45.1 and CD45.2 C57BL/6 mice in the San Raffaele Scientific Institute animal research facility. All mice were maintained in a specific pathogen–free animal facility with a 12-hour dark/12-hour light cycle and standardized temperature (22° ± 2°C) and humidity (55 ± 5%). All experiments and procedures were performed according to protocols approved by the Institutional Animal Care and Use Committee (IACUC) at San Raffaele Hospital animal facilities (IACUC number: 979, 1136, 1291, 1403) and authorized by the Italian Ministry of Health and local authorities according to the Italian law.

Statistical analyses

LME models were estimated to evaluate treatment and time (if present) effects, entered as main fixed effects and in interaction, on the outcome variable, specifying random-effect terms on experimental unit or experiment ID to address dependency issues arising from the experimental design and properly model heterogeneity in the data. Random-effect terms (e.g., on experimental session and administration route) were also specified to account for even more complex forms of dependence structure among observations. Nonlinear mixed-effects models have been applied to examine the dynamics of biological parameters in dose-response studies specifying random-effect terms on experiment ID.

To fulfill underlying model assumptions, transformations of the outcome variable (for example, logarithmic transformation of tumor volume) were considered whenever necessary. After the estimation of LME models, post hoc analysis was conducted, allowing for pairwise comparison of treatment groups eventually at a fixed time point when needed. To account for multiplicity issues, *P* values were adjusted using Bonferroni's approach.

To account for dependency among observations deriving from the same experiment, mixed-effects Cox models were estimated to model survival outcome while accounting for both fixed (treatment) and random (experiment ID or administration route) effects. Once more, the analysis was followed by post hoc pairwise comparison of treatment groups and *P* values were adjusted for multiplicity using Bonferroni's approach. LMEs and mixed-effects Cox models were estimated using R software (version 4.3.1). In all of the analyses, the significance threshold was set at 0.05. When specified in the figure legends, Mann-Whitney or Kruskal-Wallis tests with Dunn's correction were performed when comparing two or more experimental groups, respectively, with at least $n = 5$ replicates. The chi-square test was performed in fig. S10 to compare cell distribution among clusters in different treatment groups.

Supplementary Materials

The PDF file includes:
Materials and Methods
Figs. S1 to S12
Legends for tables S1 to S4
Legend for data file S1
References (*67*–*74*)

Other Supplementary Material for this manuscript includes the following:
Tables S1 to S4
Data file S1
MDAR Reproducibility Checklist

REFERENCES AND NOTES

1. U. Uslu, C. H. June, Beyond the blood: Expanding CAR T cell therapy to solid tumors. *Nat. Biotechnol.* **43**, 506–515 (2025).
2. F. Rossari, F. Birocchi, L. Naldini, N. Coltella, Gene-based delivery of immune-activating cytokines for cancer treatment. *Trends Mol. Med.* **29**, 329–342 (2023).
3. M. De Palma, R. Mazzieri, L. S. Politi, F. Pucci, E. Zonari, G. Sitia, S. Mazzoleni, D. Moi, M. A. Venneri, S. Indraccolo, A. Falini, L. G. Guidotti, R. Galli, L. Naldini, Tumor-targeted interferon-α delivery by Tie2-expressing monocytes inhibits tumor growth and metastasis. *Cancer Cell* **14**, 299–311 (2008).
4. M. A. Venneri, M. D. Palma, M. Ponzoni, F. Pucci, C. Scielzo, E. Zonari, R. Mazzieri, C. Doglioni, L. Naldini, Identification of proangiogenic TIE2-expressing monocytes (TEMs) in human peripheral blood and cancer. *Blood* **109**, 5276–5285 (2007).
5. B. Gentner, I. Visigalli, H. Hiramatsu, E. Lechman, S. Ungari, A. Giustacchini, G. Schira, M. Amendola, A. Quattrini, S. Martino, A. Orlacchio, J. E. Dick, A. Biffi, L. Naldini, Identification of hematopoietic stem cell–specific miRNAs enables gene therapy of globoid cell leukodystrophy. *Sci. Transl. Med.* **2**, 58ra84 (2010).
6. G. Escobar, D. Moi, A. Ranghetti, P. Ozkal-Baydin, M. L. Squadrito, A. Kajaste-Rudnitski, A. Bondanza, B. Gentner, M. De Palma, R. Mazzieri, L. Naldini, Genetic engineering of hematopoiesis for targeted IFN-α delivery inhibits breast cancer progression. *Sci. Transl. Med.* **6**, 217ra3 (2014).
7. F. Birocchi, M. Cusimano, F. Rossari, S. Beretta, P. M. V. Rancoita, A. Ranghetti, S. Colombo, B. Costa, P. Angel, F. Sanvito, M. Callea, R. Norata, L. Chaabane, T. Canu, A. Spinelli, M. Genua, R. Ostuni, I. Merelli, N. Coltella, L. Naldini, Targeted inducible delivery of immunoactivating cytokines reprograms glioblastoma microenvironment and inhibits growth in mouse models. *Sci. Transl. Med.* **14**, eabl4106 (2022).
8. G. Escobar, L. Barbarossa, G. Barbiera, M. Norelli, M. Genua, A. Ranghetti, T. Plati, B. Camisa, C. Brombin, D. Cittaro, A. Annoni, A. Bondanza, R. Ostuni, B. Gentner, L. Naldini, Interferon gene therapy reprograms the leukemia microenvironment inducing protective immunity to multiple tumor antigens. *Nat. Commun.* **9**, 2896 (2018).
9. K. Woroniecka, P. Chongsathidkiet, K. Rhodin, H. Kemeny, C. Dechant, S. H. Farber, A. A. Elsamadicy, X. Cui, S. Koyama, C. Jackson, L. J. Hansen, T. M. Johanns, L. Sanchez-Perez, V. Chandramohan, Y.-R. A. Yu, D. D. Bigner, A. Giles, P. Healy, G. Dranoff, K. J. Weinhold, G. P. Dunn, P. E. Fecci, T-cell exhaustion signatures vary with tumor type and are severe in glioblastoma. *Clin. Cancer Res.* **24**, 4175–4186 (2018).
10. N. Ochocka, P. Segit, K. A. Walentynowicz, K. Wojnicki, S. Cyranowski, J. Swatler, J. Mieczkowski, B. Kaminska, Single-cell RNA sequencing reveals functional heterogeneity of glioma-associated brain macrophages. *Nat. Commun.* **12**, 1151 (2021).
11. S. J. Bagley, A. S. Desai, G. P. Linette, C. H. June, D. M. O'Rourke, CAR T-cell therapy for glioblastoma: Recent clinical advances and future challenges. *Neuro Oncol.* **20**, 1429–1438 (2018).
12. B. Costa, M. N. C. Fletcher, P. Boskovic, E. L. Ivanova, T. Eisemann, S. Lohr, L. Bunse, M. Löwer, S. Burchard, A. Korshunov, N. Coltella, M. Cusimano, L. Naldini, H. K. Liu, M. Platten, B. Radlwimmer, P. Angel, H. Peterziel, A set of cell lines derived from a genetic murine glioblastoma model recapitulates molecular and morphological characteristics of human tumors. *Cancers* **13**, 230 (2021).
13. H. Du, K. Hirabayashi, S. Ahn, N. P. Kren, S. A. Montgomery, X. Wang, K. Tiruthani, B. Mirlekar, D. Michaud, K. Greene, S. G. Herrera, Y. Xu, C. Sun, Y. Chen, X. Ma, C. R. Ferrone, Y. Pylayeva-Gupta, J. J. Yeh, R. Liu, B. Savoldo, S. Ferrone, G. Dotti, Antitumor responses in the absence of toxicity in solid tumors by targeting B7-H3 via chimeric antigen receptor T cells. *Cancer Cell* **35**, 221–237.e8 (2019).
14. R. G. Majzner, J. L. Theruvath, A. Nellan, S. Heitzeneder, Y. Cui, C. W. Mount, S. P. Rietberg, M. H. Linde, P. Xu, C. Rota, E. Sotillo, L. Labanieh, D. W. Lee, R. J. Orentas, D. S. Dimitrov, Z. Zhu, B. S. Croix, A. Delaidelli, A. Sekunova, E. Bonvini, S. S. Mitra, M. M. Quezado, R. Majeti, M. Monje, P. H. B. Sorensen, J. M. Maris, C. L. Mackall, CAR T cells targeting B7-H3, a pan-cancer antigen, demonstrate potent preclinical activity against pediatric solid tumors and brain tumors. *Clin. Cancer Res.* **25**, 2560–2574 (2019).
15. M. Delville, T. Soheili, F. Bellier, A. Durand, A. Denis, C. Lagresle-Peyrou, M. Cavazzana, I. Andre-Schmutz, E. Six, A nontoxic transduction enhancer enables highly efficient lentiviral transduction of primary murine T cells and hematopoietic stem cells. *Mol. Ther. Methods Clin. Dev.* **10**, 341–347 (2018).
16. C. Petrillo, L. G. Thorne, G. Unali, G. Schiroli, A. M. S. Giordano, F. Piras, I. Cuccovillo, S. J. Petit, F. Ahsan, M. Noursadeghi, S. Clare, P. Genovese, B. Gentner, L. Naldini, G. J. Towers, A. Kajaste-Rudnitski, Cyclosporine H overcomes innate immune restrictions to improve lentiviral transduction and gene editing in human hematopoietic stem cells. *Cell Stem Cell* **23**, 820–832.e9 (2018).
17. S. Park, M. V. Maus, B. D. Choi, CAR-T cell therapy for the treatment of adult high-grade gliomas. *NPJ Precis. Oncol.* **8**, 279 (2024).
18. J. T. Sockolosky, E. Trotta, G. Parisi, L. Picton, L. L. Su, A. C. Le, A. Chhabra, S. L. Silveria, B. M. George, I. C. King, M. R. Tiffany, K. Jude, L. V. Sibener, D. Baker, J. A. Shizuru, A. Ribas, J. A. Bluestone, K. C. Garcia, Selective targeting of engineered T cells using orthogonal IL-2 cytokine-receptor complexes. *Science* **359**, 1037–1042 (2018).
19. Q. Zhang, M. E. Hresko, L. K. Picton, L. Su, M. J. Hollander, S. Nunez-Cruz, Z. Zhang, C. A. Assenmacher, J. T. Sockolosky, K. C. Garcia, M. C. Milone, A human orthogonal IL-2 and IL-2Rβ system enhances CAR T cell expansion and antitumor activity in a murine model of leukemia. *Sci. Transl. Med.* **13**, eabg6986 (2021).
20. P. J. Aspuria, S. Vivona, M. Bauer, M. Semana, N. Ratti, S. McCauley, R. Riener, R. de Waal Malefyt, D. Rokkam, J. Emmerich, R. A. Kastelein, P. J. Lupardus, M. Oft, An orthogonal IL-2 and IL-2Rβ system drives persistence and activation of CAR T cells and clearance of bulky lymphoma. *Sci. Transl. Med.* **13**, eabg7565 (2021).
21. J. H. Levine, E. F. Simonds, S. C. Bendall, K. L. Davis, E. D. Amir, M. D. Tadmor, O. Litvin, H. G. Fienberg, A. Jager, E. R. Zunder, R. Finck, A. L. Gedman, I. Radtke, J. R. Downing, D. Pe'er, G. P. Nolan, Data-driven phenotypic dissection of AML reveals progenitor-like cells that correlate with prognosis. *Cell* **162**, 184–197 (2015).
22. C. J. Sailer, Y. Hong, A. Dahal, A. T. Ryan, S. Mir, S. A. Gerber, P. M. Reagan, M. Kim, PD-1^{Hi} CAR-T cells provide superior protection against solid tumors. *Front. Immunol.* **14**, 1187850 (2023).
23. Y. Simoni, E. Becht, M. Fehlings, C. Y. Loh, S.-L. Koo, K. W. W. Teng, J. P. S. Yeong, R. Nahar, T. Zhang, H. Kared, K. Duan, N. Ang, M. Poidinger, Y. Y. Lee, A. Larbi, A. J. Khng, E. Tan, C. Fu, R. Mathew, M. Teo, W. T. Lim, C. K. Toh, B.-H. Ong, T. Koh, A. M. Hillmer, A. Takano, T. K. H. Lim, E. H. Tan, W. Zhai, D. S. W. Tan, I. B. Tan, E. W. Newell, Bystander CD8$^+$ T cells are abundant and phenotypically distinct in human tumour infiltrates. *Nature* **557**, 575–579 (2018).
24. R. Bill, P. Wirapati, M. Messemaker, W. Roh, B. Zitti, F. Duval, M. Kiss, J. C. Park, T. M. Saal, J. Hoelzl, D. Tarussio, F. Benedetti, S. Tissot, L. Kandalaft, M. Varrone, G. Ciriello, T. A. McKee, Y. Monnier, M. Mermod, E. M. Blaum, I. Gushterova, A. L. K. Gonye, N. Hacohen, G. Getz, T. R. Mempel, A. M. Klein, R. Weissleder, W. C. Faquin, P. M. Sadow, D. Lin, S. I. Pai, M. Sade-Feldman, M. J. Pittet, CXCL9:SPP1 macrophage polarity identifies a network of cellular programs that control human cancers. *Science* **381**, 515–524 (2023).
25. N. Caronni, F. La Terza, F. M. Vittoria, G. Barbiera, L. Mezzanzanica, V. Cuzzola, S. Barresi, M. Pellegatta, P. Canevazzi, G. Dunsmore, C. Leonardi, E. Montaldo, E. Lusito, E. Dugnani, A. Citro, M. S. F. Ng, M. Schiavo Lena, D. Drago, A. Andolfo, S. Brugiapaglia, A. Scagliotti, A. Mortellaro, V. Corbo, Z. Liu, A. Mondino, P. Dellabona, L. Piemonti, C. Taveggia, C. Doglioni, P. Cappello, F. Novelli, M. Iannacone, L. G. Ng, F. Ginhoux, S. Crippa, M. Falconi, C. Bonini, L. Naldini, M. Genua, R. Ostuni, IL-1β$^+$ macrophages fuel pathogenic inflammation in pancreatic cancer. *Nature* **623**, 415–422 (2023).
26. R. Browaeys, J. Gilis, C. Sang-Aram, P. De Bleser, L. Hoste, S. Tavernier, D. Lambrechts, R. Seurinck, Y. Saeys, MultiNicheNet: A flexible framework for differential cell-cell communication analysis from multi-sample multi-condition single-cell transcriptomics data. bioRxiv 544751 [Preprint] (2023). https://doi.org/10.1101/2023.06.13.544751.

27. G. Agliardi, A. R. Liuzzi, A. Hotblack, D. De Feo, N. Núñez, C. L. Stowe, E. Friebel, F. Nannini, L. Rindlisbacher, T. A. Roberts, R. Ramasawmy, I. P. Williams, B. M. Siow, M. F. Lythgoe, T. L. Kalber, S. A. Quezada, M. A. Pule, S. Tugues, K. Straathof, B. Becher, Intratumoral IL-12 delivery empowers CAR-T cell immunotherapy in a pre-clinical model of glioblastoma. *Nat. Commun.* **12**, 444 (2021).
28. B. P. Nicolet, A. Guislain, F. P. J. van Alphen, R. Gomez-Eerland, T. N. M. Schumacher, M. van den Biggelaar, M. C. Wolkers, CD29 identifies IFN-γ–producing human $CD8^+$ T cells with an increased cytotoxic potential. *Proc. Natl. Acad. Sci. U.S.A.* **117**, 6686–6696 (2020).
29. V. Golumba-Nagy, J. Kuehle, A. A. Hombach, H. Abken, CD28-ζ CAR T cells resist TGF-β repression through IL-2 signaling, which can be mimicked by an engineered IL-7 autocrine loop. *Mol. Ther.* **26**, 2218–2230 (2018).
30. B. Hu, J. Ren, Y. Luo, B. Keith, R. M. Young, J. Scholler, Y. Zhao, C. H. June, Augmentation of antitumor immunity by human and mouse CAR T cells secreting IL-18. *Cell Rep.* **20**, 3025–3033 (2017).
31. C. R. Good, M. A. Aznar, S. Kuramitsu, P. Samareh, S. Agarwal, G. Donahue, K. Ishiyama, N. Wellhausen, A. K. Rennels, Y. Ma, L. Tian, S. Guedan, K. A. Alexander, Z. Zhang, P. C. Rommel, N. Singh, K. M. Glastad, M. W. Richardson, K. Watanabe, J. L. Tanyi, M. H. O'Hara, M. Ruella, S. F. Lacey, E. K. Moon, S. J. Schuster, S. M. Albelda, L. L. Lanier, R. M. Young, S. L. Berger, C. H. June, An NK-like CAR T cell transition in CAR T cell dysfunction. *Cell* **184**, 6081–6100.e26 (2021).
32. M. Andreatta, J. Corria-Osorio, S. Müller, R. Cubas, G. Coukos, S. J. Carmona, Interpretation of T cell states from single-cell transcriptomics data using reference atlases. *Nat. Commun.* **12**, 2965 (2021).
33. B. Van de Sande, C. Flerin, K. Davie, M. De Waegeneer, G. Hulselmans, S. Aibar, R. Seurinck, W. Saelens, R. Cannoodt, Q. Rouchon, T. Verbeiren, D. De Maeyer, J. Reumers, Y. Saeys, S. Aerts, A scalable SCENIC workflow for single-cell gene regulatory network analysis. *Nat. Protoc.* **15**, 2247–2276 (2020).
34. R. C. Lynn, E. W. Weber, E. Sotillo, D. Gennert, P. Xu, Z. Good, H. Anbunathan, J. Lattin, R. Jones, V. Tieu, S. Nagaraja, J. Granja, C. F. A. de Bourcy, R. Majzner, A. T. Satpathy, S. R. Quake, M. Monje, H. Y. Chang, C. L. Mackall, c-Jun overexpression in CAR T cells induces exhaustion resistance. *Nature* **576**, 293–300 (2019).
35. J.-C. Beltra, M. S. Abdel-Hakeem, S. Manne, Z. Zhang, H. Huang, M. Kurachi, L. Su, L. Picton, S. F. Ngiow, Y. Muroyama, V. Casella, Y. J. Huang, J. R. Giles, D. Mathew, J. Belman, M. Klapholz, H. Decaluwe, A. C. Huang, S. L. Berger, K. C. Garcia, E. J. Wherry, Stat5 opposes the transcription factor Tox and rewires exhausted $CD8^+$ T cells toward durable effector-like states during chronic antigen exposure. *Immunity* **56**, 2699–2718.e11 (2023).
36. Z. Zhao, M. Condomines, S. J. C. van der Stegen, F. Perna, C. C. Kloss, G. Gunset, J. Plotkin, M. Sadelain, Structural design of engineered costimulation determines tumor rejection kinetics and persistence of CAR T cells. *Cancer Cell* **28**, 415–428 (2015).
37. A. E. Doan, K. P. Mueller, A. Y. Chen, G. T. Rouin, Y. Chen, B. Daniel, J. Lattin, M. Markovska, B. Mozarsky, J. Arias-Umana, R. Hapke, I.-Y. Jung, A. Wang, P. Xu, D. Klysz, G. Zuern, M. Bashti, P. J. Quinn, Z. Miao, K. Sandor, W. Zhang, G. M. Chen, F. Ryu, M. Logun, J. Hall, K. Tan, S. A. Grupp, S. E. McClory, C. A. Lareau, J. A. Fraietta, E. Sotillo, A. T. Satpathy, C. L. Mackall, E. W. Weber, FOXO1 is a master regulator of memory programming in CAR T cells. *Nature* **629**, 211–218 (2024).
38. Z. Zhu, G. Lou, X.-L. Teng, H. Wang, Y. Luo, W. Shi, K. Yihunie, S. Hao, K. DeGolier, C. Liao, H. Huang, Q. Zhang, T. Fry, T. Wang, C. Yao, T. Wu, FOXP1 and KLF2 reciprocally regulate checkpoints of stem-like to effector transition in CAR T cells. *Nat. Immunol.* **25**, 117–128 (2024).
39. B. Wu, X. Zhang, H.-C. Chiang, H. Pan, B. Yuan, P. Mitra, L. Qi, H. Simonyan, C. N. Young, E. Yvon, Y. Hu, N. Zhang, R. Li, RNA polymerase II pausing factor NELF in $CD8^+$ T cells promotes antitumor immunity. *Nat. Commun.* **13**, 2155 (2022).
40. Y. Pritykin, J. van der Veeken, A. R. Pine, Y. Zhong, M. Sahin, L. Mazutis, D. Pe'er, A. Y. Rudensky, C. S. Leslie, A unified atlas of CD8 T cell dysfunctional states in cancer and infection. *Mol. Cell* **81**, 2477–2493.e10 (2021).
41. N. Jain, Z. Zhao, J. Feucht, R. Koche, A. Iyer, A. Dobrin, J. Mansilla-Soto, J. Yang, Y. Zhan, M. Lopez, G. Gunset, M. Sadelain, TET2 guards against unchecked BATF3-induced CAR T cell expansion. *Nature* **615**, 315–322 (2023).
42. A. Elewaut, G. Estivill, F. Bayerl, L. Castillon, M. Novatchkova, E. Pottendorfer, L. Hoffmann-Haas, M. Schönlein, T. V. Nguyen, M. Lauss, F. Andreatta, M. Vulin, I. Krecioch, J. Bayerl, A.-M. Pedde, N. Fabre, F. Holstein, S. M. Cronin, S. Rieser, D. D. Laniti, D. Barras, G. Coukos, C. Quek, X. Bai, M. Muñoz i Ordoño, T. Wiesner, J. Zuber, G. Jönsson, J. P. Böttcher, S. Vanharanta, A. C. Obenauf, Cancer cells impair monocyte-mediated T cell stimulation to evade immunity. *Nature* **637**, 716–725 (2025).
43. B. S. Parker, J. Rautela, P. J. Hertzog, Antitumour actions of interferons: Implications for cancer therapy. *Nat. Rev. Cancer* **16**, 131–144 (2016).
44. T. Kerzel, G. Giacca, S. Beretta, C. Bresesti, M. Notaro, G. M. Scotti, C. Balestrieri, T. Canu, M. Redegalli, F. Pedica, M. Genua, R. Ostuni, A. Kajaste-Rudnitski, M. Oshima, G. Tonon, I. Merelli, L. Aldrighetti, P. Dellabona, N. Coltella, C. Doglioni, P. M. V. Rancoita, F. Sanvito, L. Naldini, M. L. Squadrito, In vivo macrophage engineering reshapes the tumor microenvironment leading to eradication of liver metastases. *Cancer Cell* **41**, 1892–1910.e10 (2023).
45. E. Duong, T. B. Fessenden, E. Lutz, T. Dinter, L. Yim, S. Blatt, A. Bhutkar, K. D. Wittrup, S. Spranger, Type I interferon activates MHC class I-dressed $CD11b^+$ conventional dendritic cells to promote protective anti-tumor $CD8^+$ T cell immunity. *Immunity* **55**, 308–323.e9 (2022).
46. L. Evgin, A. L. Huff, P. Wongthida, J. Thompson, T. Kottke, J. Tonne, M. Schuelke, K. Ayasoufi, C. B. Driscoll, K. G. Shim, P. Reynolds, D. D. Monie, A. J. Johnson, M. Coffey, S. L. Young, G. Archer, J. Sampson, J. Pulido, L. S. Perez, R. Vile, Oncolytic virus-derived type I interferon restricts CAR T cell therapy. *Nat. Commun.* **11**, 3187 (2020).
47. T. S. Sumida, S. Dulberg, J. C. Schupp, M. R. Lincoln, H. A. Stillwell, P. P. Axisa, M. Comi, A. Unterman, N. Kaminski, A. Madi, V. K. Kuchroo, D. A. Hafler, Type I interferon transcriptional network regulates expression of coinhibitory receptors in human T cells. *Nat. Immunol.* **23**, 632–642 (2022).
48. M. Morotti, A. J. Grimm, H. C. Hope, M. Arnaud, M. Desbuisson, N. Rayroux, D. Barras, M. Masid, B. Murgues, B. S. Chap, M. Ongaro, I. A. Rota, C. Ronet, A. Minasyan, J. Chiffelle, S. B. Lacher, S. Bobisse, C. Murgues, E. Ghisoni, K. Ouchen, R. Bou Mjahed, F. Benedetti, N. Abdellaoui, R. Turrini, P. O. Gannon, K. Zaman, P. Mathevet, L. Lelievre, I. Crespo, M. Conrad, G. Verdeil, L. E. Kandalaft, J. Dagher, J. Corria-Osorio, M.-A. Doucey, P.-C. Ho, A. Harari, N. Vannini, J. P. Böttcher, D. Dangaj Laniti, G. Coukos, PGE_2 inhibits TIL expansion by disrupting IL-2 signalling and mitochondrial function. *Nature* **629**, 426–434 (2024).
49. S. B. Lacher, J. Dörr, G. P. de Almeida, J. Hönninger, F. Bayerl, A. Hirschberger, A.-M. Pedde, P. Meiser, L. Ramsauer, T. J. Rudolph, N. Spranger, M. Morotti, A. J. Grimm, S. Jarosch, A. Oner, L. Gregor, S. Lesch, S. Michaelides, L. Fertig, D. Briukhovetska, L. Majed, S. Stock, D. H. Busch, V. R. Buchholz, P. A. Knolle, D. Zehn, D. Dangaj Laniti, S. Kobold, J. P. Böttcher, PGE_2 limits effector expansion of tumour-infiltrating stem-like $CD8^+$ T cells. *Nature* **629**, 417–425 (2024).
50. D. Alizadeh, R. A. Wong, S. Gholamin, M. Maker, M. Aftabizadeh, X. Yang, J. R. Pecoraro, J. D. Jeppson, D. Wang, B. Aguilar, R. Starr, C. B. Larmonier, N. Larmonier, M.-H. Chen, X. Wu, A. Ribas, B. Badie, S. J. Forman, C. E. Brown, IFNγ is critical for CAR T cell–mediated myeloid activation and induction of endogenous immunity. *Cancer Discov.* **11**, 2248–2265 (2021).
51. G. Li, J. C. Boucher, H. Kotani, K. Park, Y. Zhang, B. Shrestha, X. Wang, L. Guan, N. Beatty, D. Abate-Daga, M. L. Davila, 4-1BB enhancement of CAR T function requires NF-κB and TRAFs. *JCI Insight* **3**, e121322 (2018).
52. A. Textor, L. Grunewald, K. Anders, A. Klaus, S. Schwiebert, A. Winkler, M. Stecklum, J. Rolff, A. G. Henssen, U. E. Höpken, A. Eggert, J. H. Schulte, M. C. Jensen, T. Blankenstein, A. Künkele, CD28 co-stimulus achieves superior CAR T cell effector function against solid tumors than 4-1BB co-stimulus. *Cancers* **13**, 1050 (2021).
53. S. Srivastava, S. N. Furlan, C. A. Jaeger-Ruckstuhl, M. Sarvothama, C. Berger, K. S. Smythe, S. M. Garrison, J. M. Specht, S. M. Lee, R. A. Amezquita, V. Voillet, V. Muhunthan, S. Yechan-Gunja, S. P. S. Pillai, C. Rader, A. M. Houghton, R. H. Pierce, R. Gottardo, D. G. Maloney, S. R. Riddell, Immunogenic chemotherapy enhances recruitment of CAR-T cells to lung tumors and improves antitumor efficacy when combined with checkpoint blockade. *Cancer Cell* **39**, 193–208.e10 (2021).
54. G. Guzman, K. Pellot, M. R. Reed, A. Rodriguez, CAR T-cells to treat brain tumors. *Brain Res. Bull.* **196**, 76–98 (2023).
55. R. G. Majzner, S. Ramakrishna, K. W. Yeom, S. Patel, H. Chinnasamy, L. M. Schultz, R. M. Richards, L. Jiang, V. Barsan, R. Mancusi, A. C. Geraghty, Z. Good, A. Y. Mochizuki, S. M. Gillespie, A. M. S. Toland, J. Mahdi, A. Reschke, E. H. Nie, I. J. Chau, M. C. Rotiroti, C. W. Mount, C. Baggott, S. Mavroukakis, E. Egeler, J. Moon, C. Erickson, S. Green, M. Kunicki, M. Fujimoto, Z. Ehlinger, W. Reynolds, S. Kurra, K. E. Warren, S. Prabhu, H. Vogel, L. Rasmussen, T. T. Cornell, S. Partap, P. G. Fisher, C. J. Campen, M. G. Filbin, G. Grant, B. Sahaf, K. L. Davis, S. A. Feldman, C. L. Mackall, M. Monje, GD2-CAR T cell therapy for H3K27M-mutated diffuse midline gliomas. *Nature* **603**, 934–941 (2022).
56. C. E. Brown, J. C. Hibbard, D. Alizadeh, M. S. Blanchard, H. M. Natri, D. Wang, J. R. Ostberg, B. Aguilar, J. R. Wagner, J. A. Paul, R. Starr, R. A. Wong, W. Chen, N. Shulkin, M. Aftabizadeh, A. Filippov, A. Chaudhry, J. A. Ressler, J. Kilpatrick, P. Myers-McNamara, M. Chen, L. D. Wang, R. C. Rockne, J. Georges, J. Portnow, M. E. Barish, M. D'Apuzzo, N. E. Banovich, S. J. Forman, B. Badie, Locoregional delivery of IL-13Rα2-targeting CAR-T cells in recurrent high-grade glioma: A phase 1 trial. *Nat. Med.* **30**, 1001–1012 (2024).
57. M. Monje, J. Mahdi, R. Majzner, K. W. Yeom, L. M. Schultz, R. M. Richards, V. Barsan, K.-W. Song, J. Kamens, C. Baggott, M. Kunicki, S. P. Rietberg, A. S. Lim, A. Reschke, S. Mavroukakis, E. Egeler, J. Moon, S. Patel, H. Chinnasamy, C. Erickson, A. Jacobs, A. K. Duh, R. Tunuguntla, D. D. Klysz, C. Fowler, S. Green, B. Beebe, C. Carr, M. Fujimoto, A. K. Brown, A.-L. G. Petersen, C. McIntyre, A. Siddiqui, N. Lepori-Bui, K. Villar, K. Pham, R. Bove, E. Musa, W. D. Reynolds, A. Kuo, S. Prabhu, L. Rasmussen, T. T. Cornell, S. Partap, P. G. Fisher, C. J. Campen, G. Grant, L. Prolo, X. Ye, B. Sahaf, K. L. Davis, S. A. Feldman, S. Ramakrishna, C. Mackall, Intravenous and intracranial GD2-CAR T cells for $H3K27M^+$ diffuse midline gliomas. *Nature* **637**, 708–715 (2025).
58. H. Meister, T. Look, P. Roth, S. Pascolo, U. Sahin, S. Lee, B. D. Hale, B. Snijder, L. Regli, V. M. Ravi, D. H. Heiland, C. L. Sentman, M. Weller, T. Weiss, Multifunctional mRNA-based CAR T cells display promising antitumor activity against glioblastoma. *Clin. Cancer Res.* **28**, 4747–4756 (2022).

59. J. Lee, M. Nicosia, J. D. Lathia, Antibody-cytokine fusion breathes new life into glioblastoma therapy. *Sci. Transl. Med.* **15**, eadh7674 (2023).
60. L. Zhang, R. A. Morgan, J. D. Beane, Z. Zheng, M. E. Dudley, S. H. Kassim, A. V. Nahvi, L. T. Ngo, R. M. Sherry, G. Q. Phan, M. S. Hughes, U. S. Kammula, S. A. Feldman, M. A. Toomey, S. P. Kerkar, N. P. Restifo, J. C. Yang, S. A. Rosenberg, Tumor-infiltrating lymphocytes genetically engineered with an inducible gene encoding interleukin-12 for the immunotherapy of metastatic melanoma. *Clin. Cancer Res.* **21**, 2278–2288 (2015).
61. R. E. O'Cearbhaill, J. H. Park, E. F. Halton, C. R. Diamonte, E. Mead, Y. Lakhman, P. Kane, I. C. Riviere, R. J. Brentjens, A phase I clinical trial of autologous chimeric antigen receptor (CAR) T cells genetically engineered to secrete IL-12 and to target the MUC16ecto antigen in patients (pts) with MUC16ecto+ recurrent high-grade serous ovarian cancer (HGSOC). *Gynecol. Oncol.* **159**, 42 (2020).
62. S. Kaczanowska, D. W. Beury, V. Gopalan, A. K. Tycko, H. Qin, M. E. Clements, J. Drake, C. Nwanze, M. Murgai, Z. Rae, W. Ju, K. A. Alexander, J. Kline, C. F. Contreras, K. M. Wessel, S. Patel, S. Hannenhalli, M. C. Kelly, R. N. Kaplan, Genetically engineered myeloid cells rebalance the core immune suppression program in metastasis. *Cell* **184**, 2033–2052.e21 (2021).
63. A. Ghasemi, A. Martinez-Usatorre, L. Li, M. Hicham, A. Guichard, R. Marcone, N. Fournier, B. Torchia, D. Martinez Bedoya, S. Davanture, M. Fernández-Vaquero, C. Fan, J. Janzen, Y. Mohammadzadeh, R. Genolet, N. Mansouri, M. Wenes, D. Migliorini, M. Heikenwalder, M. De Palma, Cytokine-armed dendritic cell progenitors for antigen-agnostic cancer immunotherapy. *Nat. Cancer* **5**, 240–261 (2023).
64. F. Farina, B. Gentner, G. Finocchiaro, M. Eoli, A. Capotondo, E. Anghileri, M. Barcella, V. Brambilla, M. G. Carrabba, V. Cuccarini, Q. G. D'Alessandris, F. Di Meco, V. Ferla, P. Ferroli, F. Gagliardi, F. G. Legnani, S. Mazzoleni, A. Olivi, R. Pallini, M. Saini, K. Mullen, L. Naldini, C. Russo, F. Ciceri, Genetic engineering of hematopoietic progenitor stem cells for targeted IFN-α immunotherapy reprogramming the solid tumor microenvironment: A first-in-man study in glioblastoma multiforme (NCT03866109). *Blood* **142**, 4850 (2023).
65. S. J. Bagley, M. Logun, J. A. Fraietta, X. Wang, A. S. Desai, L. J. Bagley, A. Nabavizadeh, D. Jarocha, R. Martins, E. Maloney, L. Lledo, C. Stein, A. Marshall, R. Leskowitz, J. K. Jadlowsky, S. Christensen, B. S. Oner, G. Plesa, A. Brennan, V. Gonzalez, F. Chen, Y. Sun, W. Gladney, D. Barrett, M. P. Nasrallah, W.-T. Hwang, G.-L. Ming, H. Song, D. L. Siegel, C. H. June, E. O. Hexner, Z. A. Binder, D. M. O'Rourke, Intrathecal bivalent CAR T cells targeting EGFR and IL13Rα2 in recurrent glioblastoma: Phase 1 trial interim results. *Nat. Med.* **30**, 1320–1329 (2024).
66. B. D. Choi, E. R. Gerstner, M. J. Frigault, M. B. Leick, C. W. Mount, L. Balaj, S. Nikiforow, B. S. Carter, W. T. Curry, K. Gallagher, M. V. Maus, Intraventricular CARv3-TEAM-E T cells in recurrent glioblastoma. *N. Engl. J. Med.* **390**, 1290–1298 (2024).
67. J. N. Kochenderfer, Z. Yu, D. Frasheri, N. P. Restifo, S. A. Rosenberg, Adoptive transfer of syngeneic T cells transduced with a chimeric antigen receptor that recognizes murine CD19 can eradicate lymphoma and normal B cells. *Blood* **116**, 3875–3886 (2010).
68. J. N. Brudno, N. Lam, D. Vanasse, Y. W. Shen, J. J. Rose, J. Rossi, A. Xue, A. Bot, N. Scholler, L. Mikkilineni, M. Roschewski, R. Dean, R. Cachau, P. Youkharibache, R. Patel, B. Hansen, D. F. Stroncek, S. A. Rosenberg, R. E. Gress, J. N. Kochenderfer, Safety and feasibility of anti-CD19 CAR T cells with fully human binding domains in patients with B-cell lymphoma. *Nat. Med.* **26**, 270–280 (2020).
69. M. De Palma, L. Naldini, Transduction of a gene expression cassette using advanced generation lentiviral vectors. *Methods Enzymol.* **346**, 514–529 (2002).
70. S. Ferrari, A. Jacob, S. Beretta, G. Unali, L. Albano, V. Vavassori, D. Cittaro, D. Lazarevic, C. Brombin, F. Cugnata, A. Kajaste-Rudnitski, I. Merelli, P. Genovese, L. Naldini, Efficient gene editing of human long-term hematopoietic stem cells validated by clonal tracking. *Nat. Biotechnol.* **38**, 1298–1308 (2020).
71. G. Alvisi, S. Puccio, R. Roychoudhuri, C. Scirgolea, E. Lugli, High-dimensional single-cell profiling of tumor-infiltrating $CD4^+$ regulatory T cells. *Methods Mol. Biol.* **2559**, 243–257 (2023).
72. C. E. Whyte, D. J. Tumes, A. Liston, O. T. Burton, Do more with less: Improving high parameter cytometry through overnight staining. *Curr. Protoc.* **2**, e589 (2022).
73. S. Puccio, G. Grillo, G. Alvisi, C. Scirgolea, G. Galletti, E. M. C. Mazza, A. Consiglio, G. De Simone, F. Licciulli, E. Lugli, CRUSTY: A versatile web platform for the rapid analysis and visualization of high-dimensional flow cytometry data. *Nat. Commun.* **14**, 5102 (2023).
74. D. van Dijk, R. Sharma, J. Nainys, K. Yim, P. Kathail, A. J. Carr, C. Burdziak, K. R. Moon, C. L. Chaffer, D. Pattabiraman, B. Bierie, L. Mazutis, G. Wolf, S. Krishnaswamy, D. Pe'er, Recovering gene interactions from single-cell data using data diffusion. *Cell* **174**, 716–729.e27 (2018).

Acknowledgments: We thank the members of the Naldini laboratory for discussion, the IRCCS San Raffaele Hospital Flow Cytometry facility (FRACTAL), and the SR-TIGET Immune-core. We thank A. Ranghetti, S. Iaia, and L. Sergi Sergi for technical help and C. Di Serio for coordinating the University Centre for Statistics in the Biomedical Sciences (CUSSB) support. **Funding:** This work was supported by grants to L.N. from the Italian Association for Cancer Research (AIRC; IG 20309 and IG 28749) and from the Louis-Jeantet Foundation through the 2019 Jeantet-Collen Prize for Translational Medicine. F.R. and F.B. conducted this study as partial fulfillment of their PhD in Molecular Medicine, International PhD School, Vita-Salute San Raffaele University.
Author contributions: Conceptualization: F.R., G.A., N.C., and L.N. Methodology: F.R., G.A., S.B., M.G., R.O., I.M., C.B., and P.M.V.R. Investigation: F.R., G.A., N.C., M.C., S.B., F.B., D.I.A., O.V., T.C., G.O., A.A., B.G., and M.L.S. Visualization: F.R., G.A., and S.B. Funding acquisition: L.N. Project administration: N.C. and L.N. Supervision: N.C. and L.N. Writing—original draft: F.R., G.A., N.C., and L.N. Writing—review and editing: F.R., G.A., N.C., L.N., F.B., B.G., M.L.S., R.O., and I.M.
Competing interests: L.N., N.C., B.G., F.R., and G.A. are inventors on patents on miRNA-regulated LV technology and targeted gene delivery into the TME, filed by the San Raffaele Scientific Institute and the Telethon Foundation. L.N. and B.G. own equity and are founders and advisors of Genenta Science, a biotechnology company that licensed TEM-mediated IFN gene therapy and develops its clinical applications. All other authors declare that they have no competing interests. **Data and materials availability:** All data associated with this study are present in the paper or the Supplementary Materials. scRNA-seq data are available in the Gene Expression Omnibus under the accession number GSE259346. The code used for the analyses of scRNA-seq data is available at http://bioinfotiget.it/gitlab/custom/rossari_scitramed_2025/. Materials can be made available upon signing a material transfer agreement with standard provisions. Some restrictions may apply on the use of materials involving Tie2–IFN-α gene therapy, except for research aimed at reproducing the findings reported in the paper, according to a licensing agreement with Genenta Science.

Submitted 28 February 2024
Resubmitted 28 January 2025
Accepted 7 May 2025
Published 2 July 2025
10.1126/scitranslmed.ado9511